CrystEngComm

HIGHLIGHT

View Article Online
View Journal | View Issue

Cite this: *CrystEngComm*, 2017, **19**, 4646

Experimental and theoretical investigations of the gas adsorption sites in rht-metal–organic frameworks

Tony Pham, * Katherine A. Forrest, Douglas M. Franz and Brian Space *

Received 2nd June 2017,
Accepted 18th July 2017

DOI: 10.1039/c7ce01032j

rsc.li/crystengcomm

rht-metal–organic frameworks (MOFs) represent a highly popular class of MOFs in the world of porous crystalline materials. MOFs belonging to this family consist of M^{2+} ions coordinated to hexatopic organic linkers containing three coplanar isophthalate-based moieties. **rht**-MOFs are a promising platform of MOFs because they display open-metal sites through the $[M_2(O_2CR)_4]$ clusters, high surface areas, and tunable pore sizes and chemical functionalities. They have been shown to exhibit high uptake for various energy-related gases, such as H_2 and CO_2. Detailed insights into the gas sorption mechanisms and binding sites in these MOFs can be made by way of experimental techniques, including neutron powder diffraction (NPD) and inelastic neutron scattering (INS), and theoretical methods, such as Monte Carlo (MC) simulations and electronic structure calculations. In this highlight, we review the important experimental and theoretical studies that have been performed to investigate the favorable gas sorption sites in these MOFs. A better understanding of the gas sorption mechanisms in **rht**-MOFs and related structures can allow for the rational design of new materials that are tailored for specific applications.

I. Introduction

Metal–organic frameworks (MOFs) are solid crystalline materials that are synthesized from metal ions and organic ligands (or "linkers").[1] These two components combine together in a self-assembly process to create a three-dimensional framework that is often porous. The pores of these materials can be used to sorb guest molecules, such as H_2, CO_2, CH_4, and N_2. Because of their porous nature, MOFs have been considered to be promising candidates for a variety of gas sorption applications, such as H_2 storage,[2] CH_4 storage,[3] and CO_2 capture and sequestration.[4] MOFs have the ability to capture a large amount of sorbate molecules within their pores and release them freely through adjustments in

Department of Chemistry, University of South Florida, 4202 East Fowler Avenue, CHE205, Tampa, FL 33620-5250, USA. E-mail: tpham4@mail.usf.edu, brian.b.space@gmail.com

Tony Pham

Tony Pham was born and raised in St. Petersburg, Florida. He obtained his B.S. degree at the University of South Florida (USF) in 2008. In 2015, he received his Ph.D. in Computational Chemistry at USF working under the advisement of Professor Brian Space. His research involves the modeling of gas adsorption and separation in various porous materials, including metal–organic frameworks (MOFs). As a Postdoctoral Researcher at USF, he remains working closely with Dr. Space's research group and experimental collaborators to elucidate the gas adsorption mechanisms in MOFs using sophisticated modeling techniques.

Katherine A. Forrest

Katherine A. Forrest was born in San Francisco, California and raised in Clearwater, Florida. She received a B.S. degree in Chemistry at the University of South Florida (USF) in 2008. As a Ph.D. candidate, she works under Professor Brian Space performing research in the field of computational chemistry at USF. The main focus of her current research regards metal–organic frameworks (MOFs) for gas storage, separations, and catalysis. Specifically, her work involves the implementation of computational methods to understand the atomistic behavior in MOFs in collaboration with experimental chemists.

thermodynamic conditions. MOFs are highly tunable, as a number of different structures can be synthesized by changing the metal ion and/or organic ligand.[5] Indeed, over 20 000 different MOF structures with distinct pore sizes, topologies, and chemical functionalities have been synthesized and reported in the literature.[6]

The **rht**-MOF platform is a highly popular class of MOFs that exists in the literature.[7–40] These MOFs are synthesized by combining metal ions in the 2+ oxidation state with hexatopic ligands that contain three coplanar isophthalate-based moieties. Each carboxylate group of the ligand coordinates to M^{2+} ions (usually Cu^{2+}) to form the square metal paddlewheel, $[M_2(O_2CR)_4]$, molecular building block (MBB). A total of 48 carboxylate groups are connected to M^{2+} ions to form 12 paddlewheel MBBs; these MBBs are connected through the isophthalate-based components of the ligand to give rise to a cuboctahedron (cub-O_h). The center of the ligand, which typically constitutes a component with C_3 symmetry, represents a triangular building block. The points of extension from the isophthalate-based group correspond to an edge of the cub-O_h. There are 24 edges of a cub-O_h and each edge is connected to triangular building blocks (*i.e.*, the central components of the triisophthalate-based ligands) to give the (3,24)-connected **rht** net. The overall structure of **rht**-MOFs consists of three distinct porous cages: the cub-O_h, the truncated tetrahedron (T-T_d), and the truncated octahedron (T-O_h). A schematic of how **rht**-MOFs are constructed is shown in Fig. 1. Over 40 different **rht**-MOF structures have been synthesized and reported in the literature. **rht**-MOFs are a promising class of MOFs due to the presence of open-metal sites (also known as unsaturated metal centers), high surface areas, and tunable pore sizes and functionalities. They have been shown to display high uptake for a number of energy-related gases.

In addition to experimental gas sorption measurements, various experimental and theoretical studies have been performed to pinpoint the binding sites and elucidate the gas sorption mechanism in **rht**-MOFs. In general, the sorption process and nature of the binding sites in MOFs are often not well-understood. Experimental techniques to probe the binding sites in such materials typically include neutron powder diffraction (NPD) or inelastic neutron scattering (INS), while theoretical methods involve grand canonical Monte Carlo (GCMC) simulations or electronic structure calculations. In this highlight, we provide an overview of the significant experimental and theoretical studies that have been executed to investigate the sorption sites in different members of the popular **rht**-MOF platform. These studies have yielded detailed insights into the gas sorption mechanism in this class of MOFs. While this paper aims to survey a large amount of research, we apologize to any authors whose work has been omitted in this highlight due to oversight.

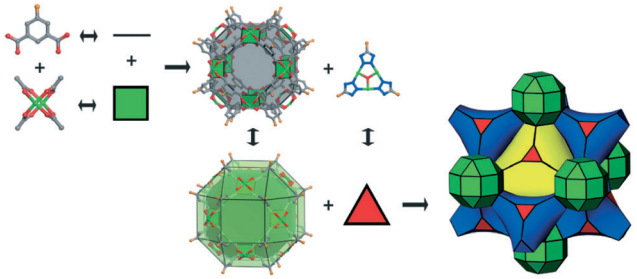

Fig. 1 A scheme showing the construction of **rht**-MOFs using **rht**-MOF-1 as an example. The isophthalate (or isophthalate-based) groups (line) combine with metal ions through the oxygen atoms to form the $[M_2(O_2CR)_4]$ MBBs (square). These components combine together to form a cub-O_h. The point of extension from each isophthalate component (*i.e.*, each edge of the cub-O_h) is connected to a component that has C_3 symmetry (triangle). The resulting topology of **rht**-MOFs consists of three distinct cages: cub-O_h (green), T-T_d (blue), and T-O_h (yellow). This figure was reproduced from ref. 25 within the guidelines provided by Wiley-VCH (Germany). Copyright 2012 Wiley-VCH (Germany).

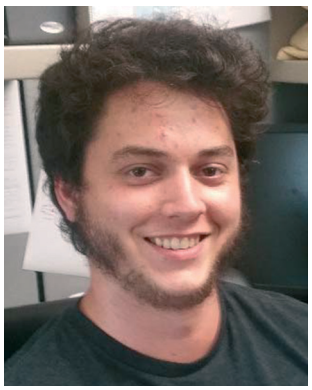

Douglas M. Franz

Douglas M. Franz was born in Seminole, Florida and received a B.S. degree in Environmental Science & Policy from the University of South Florida (USF) in 2013. He is now a Ph.D. candidate working under Professor Brian Space, with a research focus on computer simulation of guest molecules in crystalline materials, which have applications in gas adsorption, separation, and catalysis. He actively contributes toward both the application and developmental aspects of Dr. Space's research group in efforts to gain quantitative insight on submicroscopic phenomena, such as adsorption, selectivity, and diffusion of gases in metal–organic frameworks (MOFs).

Brian Space

Brian Space obtained his Ph.D. in 1992 from Boston University under the supervision of Professor David Coker. Dr. Space is an NSF Career Award winner who, after appointments at Duquesne and Princeton University, joined the University of South Florida (USF) in Tampa, where he is currently a Professor of Chemistry. His research group is primarily concerned with computer simulation of condensed phase phenomena. Current focus is the development of highly accurate potential energy functions for environmentally relevant gases, which are then employed in molecular simulations of gas adsorption within metal–organic frameworks (MOFs).

II. Experimental studies

A. Neutron powder diffraction

To the best of our knowledge, the first important experimental study that yielded insights into the binding sites in an **rht**-MOF was performed by Yan *et al.* in 2010, where the authors carried out NPD experiments of D_2 sorbed in NOTT-112.[13] NOTT-112 is an **rht**-MOF that consists of Cu^{2+} ions coordinated to 1,3,5-tris(3′,5′-dicarboxy[1,1′-biphenyl]-4-yl)benzene linkers (L4 in Fig. 2).[9] Note, an organic representation of the linkers used to synthesize all **rht**-MOFs discussed in this highlight are listed in Fig. 2. In addition, the experimental properties and selected gas sorption data for these MOFs are summarized in Tables 1 and 2, respectively. NOTT-112 was shown to have a Brunauer–Emmett–Teller (BET) surface area[41] of 3800 $m^2\ g^{-1}$ and a pore volume within the range of 1.6–1.7 $cm^3\ g^{-1}$.[9] Further, this MOF displayed an absolute H_2 uptake of 2.3 wt% at 78 K/1 bar and a zero-loading isosteric heat of adsorption (Q_{st}) value of 5.64 kJ mol^{-1} according to experimental measurements. The D_2 sorption sites observed in the MOF from NPD studies are shown in Fig. 3.

Yan *et al.* discovered two different sorption sites in NOTT-112 at a loading of 0.5 D_2/Cu (*ca.* 0.3 wt%).[13] The first of these correspond to sorption onto the Cu^{2+} ions that are located within the cub-O_h cages in the MOF (site A_1 in Fig. 3). The other sorption site was observed near the Cu^{2+} ions that are located within the T-T_d and T-O_h cages (site A_2 in Fig. 3). The authors denoted these Cu^{2+} ion sites as CuA and CuB, respectively. The refinements at this loading revealed that 85% of the D_2 molecules sorbed onto the CuA ions. This suggests that both types of Cu^{2+} ions have different affinities toward the D_2 molecule. This also indicates that the two Cu^{2+} ions that make up the copper paddlewheel units in NOTT-112 are located in unique environments in the MOF structure. Indeed, there are at least two chemically distinct M^{2+} ions in the crystal structure of all **rht**-MOFs. One type of M^{2+} ion faces toward the center of the linker and projects into the T-T_d and T-O_h cages whereas the other type faces away from the center of the linker and projects into the cub-O_h cage. This is in contrast to HKUST-1 (ref. 42) and MOF-505 (ref. 43), two prototypical MOFs containing Cu^{2+} ions coordinated to 1,3,5-benzenetricarboxylate (BTC) and 3,3′,5,5′-biphenyltetracarboxylate (BPTC) linkers, respectively, as all metal ions in these MOFs are chemically equivalent.

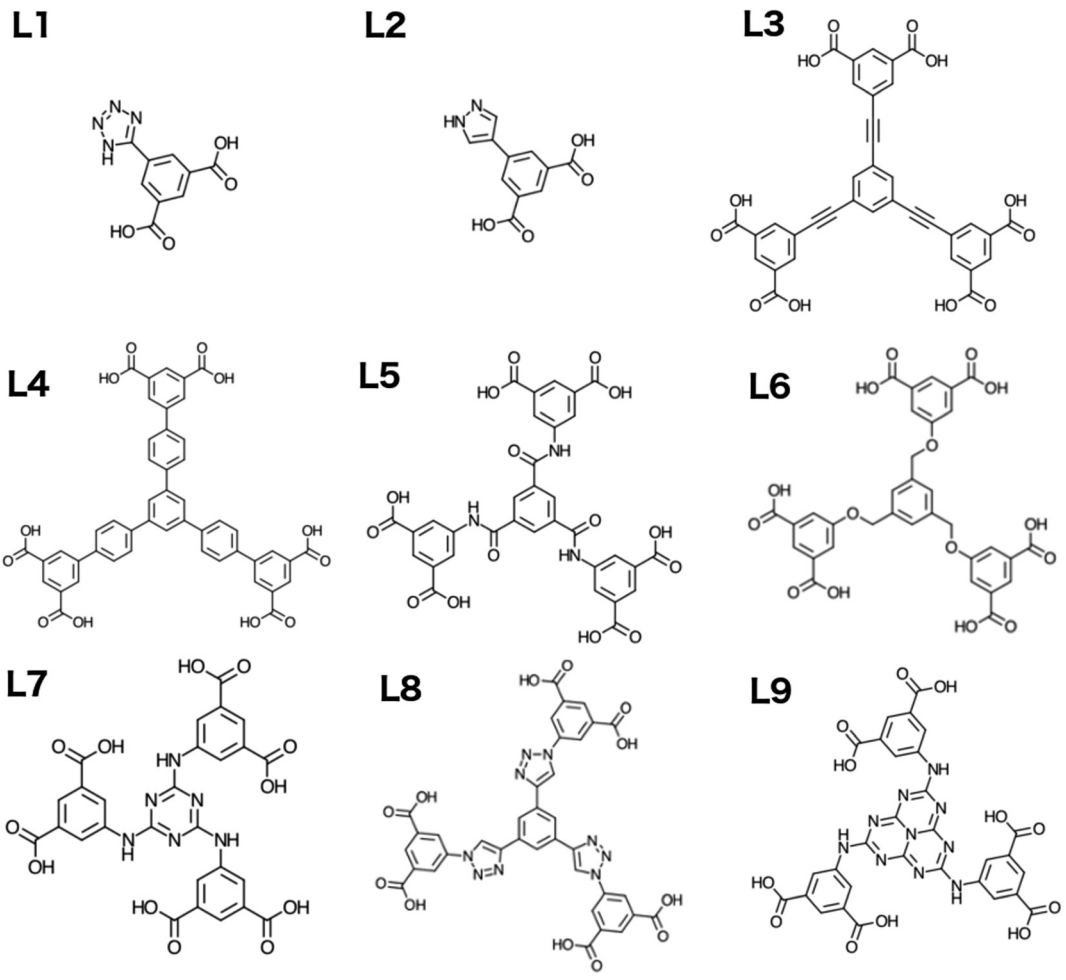

Fig. 2 Organic representations of the linkers (L1–L9) used to synthesize the **rht**-MOFs discussed in this highlight. The associated names of the **rht**-MOFs are summarized in Table 1.

Table 1 Summary of the ligand and experimental properties for the **rht**-MOFs discussed in this highlight

Name	Ligand[d]	S_L (m^2 g^{-1})	S_{BET} (m^2 g^{-1})	V_p (cm^3 g^{-1})	Density (g cm^{-3})	Reference
rht-MOF-1	L1	3223	2847	1.01	0.702	7
rht-MOF-pyr	L2	—	2133	—	0.708	35
PCN-61	L3	3500	3000 (3350)	1.36 (1.37)	0.56	12 (15)
NOTT-112	L4	—	3800	1.62	0.503	9
Cu-TPBTM	L5	3570	3160	1.27	0.627	15
rht-MOF-4a	L6	1590	1070	1.10	0.665	25
rht-MOF-7[a]	L7	2608/2170	1938/—	0.93/0.76	0.782/0.788	19/20
NTU-105[b]	L8	—	3543/3286/3120	1.33/1.41/1.29	0.598/0.589/0.578	27/28/29
rht-MOF-9[c]	L9	3070/2540	2420/2171	0.943/0.91	0.742/0.89	31/33

[a] Also known as Cu-TDPAT. [b] Also known as NOTT-122a or NU-125. [c] Also known as Cu-TDPAH. [d] Organic representations of the ligands are depicted in Fig. 2. S_L = Langmuir surface area. S_{BET} = BET surface area. V_p = Pore volume.

Table 2 Summary of the H_2, CO_2, and CH_4 sorption data for the **rht**-MOFs discussed in this highlight

Name	H_2 uptake[d] (wt%)	H_2 Q_{st}[e] (kJ mol^{-1})	CO_2 uptake[f] (mmol g^{-1})	CO_2 Q_{st}[e] (kJ mol^{-1})	CH_4 uptake[f] (mmol g^{-1})	CH_4 Q_{st}[e] (kJ mol^{-1})	Reference
rht-MOF-1	2.4 (—/1.81)	9.5	(2.57/2.43)	(32.5/29.0)	(—/0.46)	(—/19.3)	7 (20/36)
rht-MOF-pyr	1.74	—	2.96	27.7	0.50	14.2	36
PCN-61	2.25	6.36	(3.15)	21.0 (22.0)	0.79	13.79	12 (15)
NOTT-112	2.3	5.64	—	—	—	—	9
Cu-TPBTM	(2.61)	(6.6)	5.29	26.3	—	—	15 (58)
rht-MOF-4a	1.9	9.5	—	—	—	—	25
rht-MOF-7[a]	2.65/—(2.20)	8.29/—(6.77)	5.9/3.9	42.2/44.7	1.1/—	—	19/20 (48)
NTU-105[b]	2.75/2.6/2.4	6.61/6.0/5.2	4.2/4.63/4.0	36/24.5/23.8	—/0.82/0.83	—/—/15.5	27/28/29
rht-MOF-9[c]	2.72/—	6.9/—	5.83/5.18	37.9/33.8	—/1.0	—/13.8	31/33

[a] Also known as Cu-TDPAT. [b] Also known as NOTT-122a or NU-125. [c] Also known as Cu-TDPAH. [d] At 77 K/1 atm. [e] At the lowest loading evaluated. [f] At 298 K/1 atm.

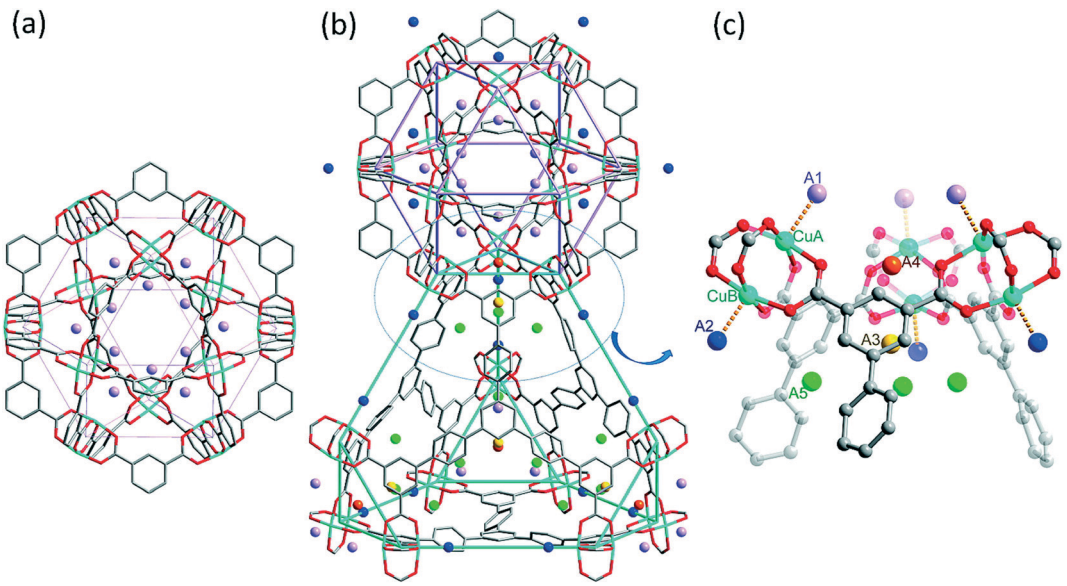

Fig. 3 Views of the D_2 molecule positions (colored spheres) in NOTT-112 as determined through neutron powder diffraction (NPD). (a) A view of the cub-O_h cage showing the D_2 molecule positions at 0.5 D_2/Cu loading. (b) A view of the cub-O_h and T-T_d cages showing the D_2 molecule positions at 2.0 D_2/Cu loading. (c) A close-up view of the corner of the T-T_d cage showing the five D_2 molecule positions (A_1, A_2, A_3, A_4, and A_5) at 2.0 D_2/Cu loading. Atom colors: C = gray, O = red, Cu = turquoise, A_1 = lavender, A_2 = blue, A_3 = yellow, A_4 = orange, A_5 = green. This figure was reproduced from ref. 13 within the guidelines provided by the American Chemical Society. Copyright 2010 American Chemical Society.

The interaction distance between the center-of-mass (COM) of the sorbed D_2 molecule and the CuA and CuB ions in NOTT-112 was found to be 2.23(1) and 2.41(1) Å, respectively, from the NPD studies.[13] The shorter CuA–COM(D_2) distance relative to that for the CuB ion indicates that the D_2 molecules exhibit a stronger interaction about the CuA ions. Thus, the CuA ions represent the most favorable sorption sites in NOTT-112. We note that the CuB–COM(D_2) distance

is very similar to that for the corresponding interaction observed in HKUST-1 through NPD studies (2.39(1) Å).[44]

The authors hypothesized that the CuA ions are more favorable than the CuB ions in the MOF because the former types are located within the small cub-O_h cages.[13] The finding that the CuA ions are preferred over the CuB ions at low loading has been supported through classical GCMC simulations of H_2 sorption in NOTT-112 that were carried out by our group recently.[45] It was discovered that the CuA ions exhibit a greater partial positive charge than the CuB ions through electronic structure calculations. This allowed for the H_2 molecules to sorb initially onto the CuA ions in simulations involving explicit many-body polarization as the sorbate molecules were more attracted to the Cu^{2+} ion having the higher partial positive charge at low loading. Thus, the simulations suggest that the differing affinities that the two types of Cu^{2+} ions have toward sorbates are due to their distinct electrostatic profiles. Overall, the NPD studies of D_2 sorption in NOTT-112 clearly demonstrated that the two Cu^{2+} ions that comprise the $[Cu_2(O_2CR)_4]$ clusters in **rht**-MOFs are chemically distinguishable and therefore results in unique binding sites about such MBBs.

At higher loadings, Yan *et al.* discovered additional D_2 binding sites in NOTT-112 from their NPD experiments.[13] These sorption sites are located in the corners of the T-T_d cages in the MOF. At 1.0 D_2/Cu loading, a third sorption site was identified between three isophthalate groups around the 3-fold axis of the triangular window connecting the cub-O_h and T-T_d cages (site A_3 in Fig. 3). A fourth sorption site was found in the region between three neighboring copper paddlewheel units at the same loading (site A_4 in Fig. 3). This site is essentially located on the other side of the triangular window from the previous site, but on the same 3-fold axis. At a loading of 1.5 D_2/Cu, a fifth sorption site was discovered, where the sorbate molecules localize near the phenyl rings of the linker in the T-T_d cages (site A_5 in Fig. 3). Note, these sorption sites within the corners of the T-T_d cages were also observed through molecular simulation studies of H_2 sorption in NOTT-112.[45]

B. Inelastic neutron scattering

INS is a valuable spectroscopic technique that is used to gain molecular level information on the H_2 sorption sites in MOFs and other porous materials.[46,47] Although NPD gives details on the crystal structure of the guest-filled material, INS provides information on the molecular excitations of H_2 sorbed at different binding sites in the host. The INS spectra for H_2 sorbed in a MOF contain a number of distinct peaks that arise from the rotational and translational excitations of the sorbate, where each transition typically corresponds to H_2 sorbed at a specific binding site in the material. Note, most of the transitions observed in the INS spectra are due to the rotational excitations of the H_2 molecule; this greatly simplifies the task of assigning peaks in the spectra. Tentative assignments of the peaks in the INS spectra can be made based on the observed neutron transfer energies, the presence of certain types and quantities of functionalities within the material, and trends within the H_2 loading amount. Such assignments can be confirmed through quantum dynamics calculations on an accurate theoretical potential energy surface.[47] To the best of our knowledge, only three **rht**-MOFs had INS studies performed on them to date: **rht**-MOF-1,[25] **rht**-MOF-4a,[25] and **rht**-MOF-7.[48]

1. rht-MOF-1. **rht**-MOF-1 represents the first reported **rht**-MOF as it was synthesized by Eddaoudi and co-workers in 2008.[7] This MOF was synthesized through a solvothermal reaction of 5-tetrazolylisophthalic acid (L1 in Fig. 2) with $Cu(NO_3)_2 \cdot 2.5H_2O$ in an *N*,*N*-dimethylformamide/ethanol solution. **rht**-MOF-1 contains trigonal $[Cu_3O(N_4CR)_3]$ MBBs linked to isophthalate groups, which in turn are coordinated to Cu^{2+} ions through the carboxylate oxygen atoms to form the copper paddlewheel clusters. Since each $[Cu_3O(N_4CR)_3]$ MBB exhibit a +1 charge, the MOF contains unbound nitrate ions to balance the charge of the cationic framework. **rht**-MOF-1 has a BET surface area of 2847 $m^2\ g^{-1}$ (Langmuir surface area is 3223 $m^2\ g^{-1}$), a pore volume of 1.01 $cm^3\ g^{-1}$, and a porosity of 75%. Furthermore, experimental gas sorption studies have shown that **rht**-MOF-1 is capable of sorbing 2.4 wt% of H_2 at 77 K/1 atm and displays a high H_2 Q_{st} value of 9.5 kJ mol^{-1} at zero coverage. The INS spectra for H_2 sorbed in this MOF were collected in 2012 by Eubank *et al.*[25] and are reproduced in Fig. 4(a).

At both loadings, a peak can be observed at approximately 9.0 meV in the INS spectra. This peak most likely corresponds to H_2 sorbing onto the Cu^{2+} ions of the copper paddlewheels on the basis of what was observed through INS measurements on other MOFs containing these MBBs.[25,49–51] Indeed, INS studies on HKUST-1 also revealed a peak near 9.0 meV in the resulting spectra.[50] Since both **rht**-MOF-1 and HKUST-1 contain $[Cu_2(O_2CR)_4]$ clusters, this peak at *ca.* 9.0 meV in the individual spectra can likely be attributed to H_2 sorbing onto such sites. This was actually confirmed through two-dimensional quantum rotation calculations for a H_2 molecule sorbed about the Cu^{2+} ion of the copper paddlewheels in both MOFs, as such calculations produced rotational levels that are near 9.0 meV for the lowest $j = 0$ to $j = 1$ transition.[50,52] Note, in the absence of a barrier to rotation, a H_2 molecule rotates freely with energy levels that are representative of a rigid rotor. The lowest $j = 0$ to $j = 1$ transition for unhindered H_2 corresponds to a value of 14.7 meV.

At 2 H_2/Cu loading, a well-defined shoulder ranging from 6.5–8.0 meV becomes apparent in the INS spectrum for **rht**-MOF-1. The authors in ref. 25 attributed this peak to H_2 sorbing onto the Cu^{2+} ions of the $[Cu_3O(N_4CR)_3]$ units in the MOF. A peak within the aforementioned range of energies was not observed in the INS spectra for HKUST-1 since these Cu_3O trimers are not present in this MOF.[50] Thus, the assignment of the 6.5–8.0 meV peak to H_2 sorbing onto the Cu^{2+} ions of the $[Cu_3O(N_4CR)_3]$ MBBs appears to be valid, especially since this was later confirmed through two-dimensional quantum rotation calculations.[52] It appears that the Cu_3O trimers become more occupied at higher loadings, which is consistent with what was observed through GCMC simulations of H_2 sorption in this MOF.

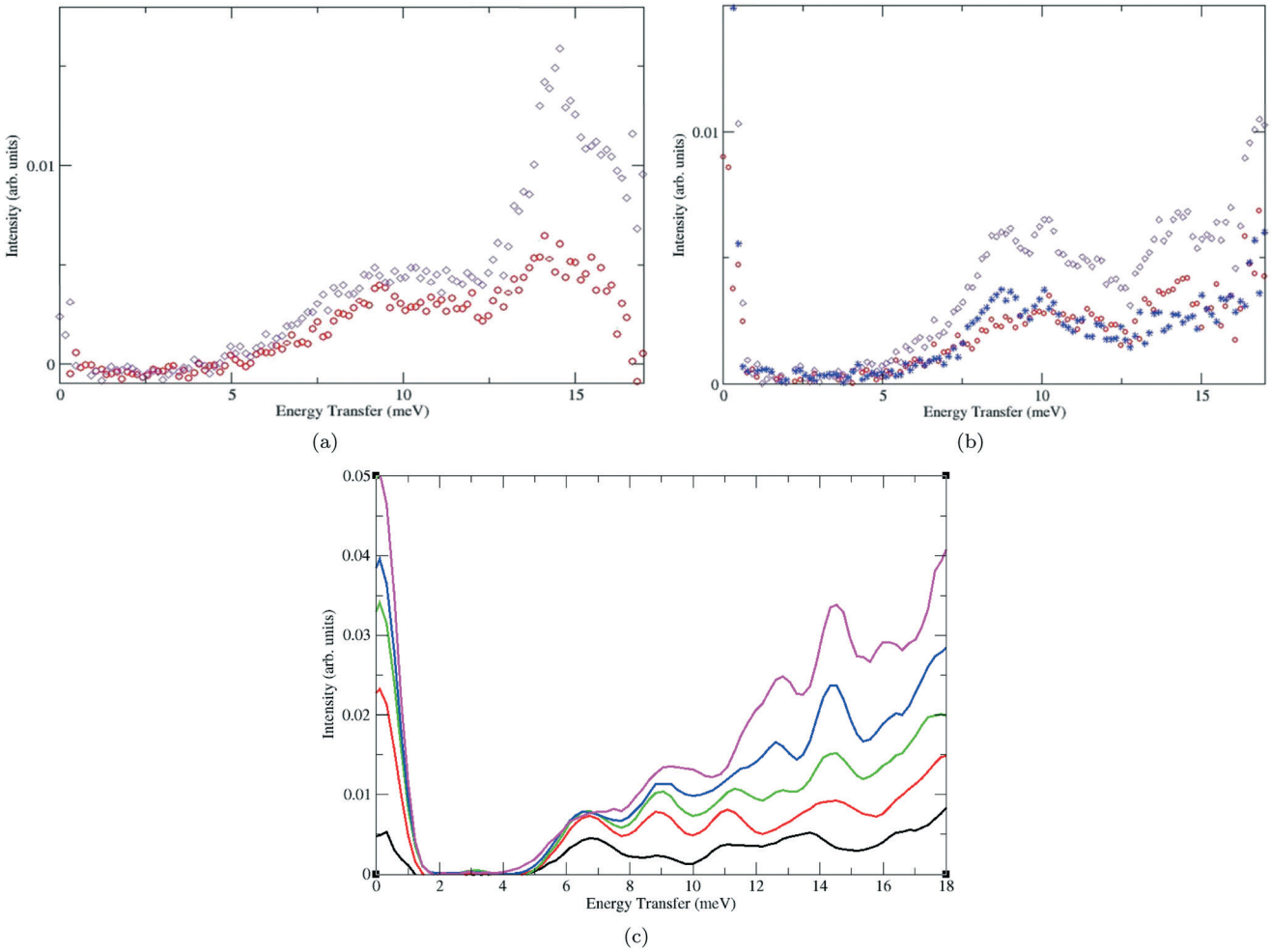

Fig. 4 Inelastic neutron scattering (INS) spectra for H_2 in (a) **rht**-MOF-1 at loadings of 1 H_2/Cu (red) and 2 H_2/Cu (violet), (b) **rht**-MOF-4a at loadings of 0.9 H_2/Cu (red) and 1.5 H_2/Cu (violet) with the difference spectrum shown in blue, and (c) **rht**-MOF-7 at loadings of 0.75 H_2 per formula unit (black), 1.5 H_2 per formula unit (red), 2.25 H_2 per formula unit (green), 3 H_2 per formula unit (blue), and 4 H_2 per formula unit (magenta). The INS spectra for **rht**-MOF-1 and **rht**-MOF-4a were reproduced from ref. 25 within the guidelines provided by Wiley-VCH (Germany). Copyright 2012 Wiley-VCH (Germany). The INS spectra for **rht**-MOF-7 were reproduced from ref. 48 within the guidelines provided by the American Chemical Society. Copyright 2014 American Chemical Society.

The INS spectra for **rht**-MOF-1 also contain a small, but noticeable peak at approximately 5.0 meV for both loadings. This peak is associated with H_2 sorbing onto the most favorable binding sites in the MOF. Note, in general, peaks that occur at lower neutron transfer energies in the INS spectra correspond to a higher barrier to rotation and therefore, a stronger interaction with the host. Two different GCMC simulations of H_2 sorption in **rht**-MOF-1 revealed that the most preferential H_2 sorption sites in the MOF are the NO_3^- counterions (see section III. A.1).[52,53] Sorption onto these nitrate ions correspond to the initial H_2 Q_{st} in the material as verified through simulations involving explicit many-body polarization.[52]

INS measurements on In-**soc**-MOF, another MOF possessing nitrate counterions,[54] also contain a peak near 5.0 meV in the resulting spectra. The authors in that reference claimed that this peak should correspond to H_2 sorbing onto the NO_3^- ions. Two-dimensional quantum rotation calculations for H_2 sorbed onto the nitrate ions in both MOFs yielded a $j = 0$ to $j = 1$ transition of 5.63 and 5.78 meV for **rht**-MOF-1 (ref. 52) and In-**soc**-MOF (ref. 55), respectively. These calculations therefore suggest that the transition occurring at about 5.0 meV in the INS spectra for both MOFs is associated with sorption onto the nitrate counterions.

A large peak can be observed at about 14.0 meV in the INS spectrum for **rht**-MOF-1 at both loadings. This peak is associated with H_2 sorbing onto the weaker binding sites in the MOF, most notably, the spacious interior of the cub-O_h cages according to GCMC simulations and attendant quantum dynamics calculations.[52] The H_2 molecules localized at such sites exhibit rigid rotor-like behavior since they give rise to transitions that are near the free rotor limit of 14.7 meV. As a result, these H_2 molecules have very low barriers to rotation within the material.

2. rht-MOF-4a. The INS spectra for H_2 sorbed in **rht**-MOF-4a at two different loadings are shown in Fig. 4(b). This MOF consists of Cu^{2+} ions coordinated to 1,3,5-tris(5-methoxy-1,3-

benzenedicarboxylate)benzene linkers (L6 in Fig. 2).[25] **rht**-MOF-4a has a BET surface area of 1070 $m^2\ g^{-1}$ (Langmuir surface area is 1590 $m^2\ g^{-1}$) and a pore volume of 0.56 $cm^3\ g^{-1}$. In addition, the MOF displays a H_2 uptake of 1.9 wt% at 77 K/1 atm and a zero-loading H_2 Q_{st} value of 9.5 kJ mol^{-1}. The flexible nature of the linker allows this MOF to exhibit a unique breathing behavior upon CO_2 sorption. Other metal analogues of **rht**-MOF-4a have also been synthesized in the same experimental reference.

As with the INS spectra for **rht**-MOF-1, a peak at about 9.0 meV can be observed in the spectrum for **rht**-MOF-4a at both loadings. This neutron transfer energy value is consistent with the lowest energy transition observed in other neutral MOFs containing copper paddlewheels.[49–51] Thus, this peak at *ca.* 9 meV should correspond to H_2 sorbing onto the Cu^{2+} ions of the copper paddlewheels in the MOF. The INS spectra for **rht**-MOF-4a also reveal a peak at around 10.5 meV. The authors in ref. 25 attributed this peak to sorption within the vicinity of the isophthalate moieties. A peak with high intensity was also observed at frequencies just below 13.5 meV, which could correspond to sorption near the alkoxy groups on the linkers. Note, unlike **rht**-MOF-1, quantum dynamics calculations were not performed on the H_2 binding sites in **rht**-MOF-4a. Thus, the assignments of the peaks at approximately 10.5 and 13.5 meV in the INS spectra for this MOF are tentative and uncorroborated.

3. rht-MOF-7. **rht**-MOF-7 (ref. 20) (also known as Cu-TDPAT (ref. 19)) is a well-known Cu^{2+}-based **rht**-MOF that was synthesized using 5,5′,5″-(1,3,5-triazine-2,4,6-triyltriimino)tris-isophthalate (L7 in Fig. 2) as the organic linker. This MOF contains N-rich regions through the secondary amine and 1,3,5-triazine groups on the linker. **rht**-MOF-7 is currently the smallest member of the **rht**-MOF family. This MOF was synthesized by two different groups,[19,20] with both groups reporting their own unique gas sorption measurements and crystal structure on the material. The gas sorption isotherms collected by the two groups are quantitatively different from each other. For example, Li *et al.* measured a CO_2 uptake of about 5.9 mmol g^{-1} at 298 K/1 atm,[19] whereas Luebke *et al.* measured an uptake of roughly 3.9 mmol g^{-1} at the same state point. Nevertheless, both groups have shown that the zero-loading CO_2 Q_{st} for **rht**-MOF-7 is greater than 42 kJ mol^{-1}, which is presently the highest within the **rht**-MOF platform.

With regards to H_2 sorption, Li *et al.* showed that **rht**-MOF-7 can sorb 2.65 wt% of H_2 at 77 K/1 atm and has an initial Q_{st} of 8.29 kJ mol^{-1}.[19] On the other hand, the corresponding values measured by Eddaoudi's group are 2.20 wt% and 6.77 kJ mol^{-1}, respectively.[48] INS measurements of H_2 sorbed in **rht**-MOF-7 revealed a number of clearly defined peaks in the spectra, which are associated with different binding sites in the MOF. The INS spectra that were collected at various loadings for this MOF are shown in Fig. 4(c). The assignments of the peaks in this spectra have been confirmed through two-dimensional quantum rotation calculations on H_2 sorbed at the binding sites that were discovered through GCMC simulations.

A relatively low energy peak can be observed in the INS spectra at around 6.8 meV. The low energy of this rotational tunnelling transition is indicative of a high barrier to rotation, and hence a very strong interaction with the host. Indeed, this peak is associated with H_2 sorbed at the most favorable sorption site in **rht**-MOF-7. The intensity of this peak appears to saturate below a loading of 1.5 H_2 per formula unit, which indicates that there is a limited number of these sites available in the MOF.

GCMC simulations of H_2 sorption in **rht**-MOF-7 revealed that the most favorable binding site in the MOF is located between two neighboring Cu^{2+} ions that project into the T-T_d and T-O_h cages,[48] named the CuB ions according to the convention by Yan *et al.*[13] An illustration of this site is shown in Fig. 5(a). The angular nature of the L7 linker causes two CuB ions to be in proximity to each other in the structure. Thus, as the H_2 molecule is sorbed in this region, it can interact with the two adjacent CuB ions simultaneously, providing for a very favorable interaction. Two-dimensional quantum rotation calculations for H_2 sorbed at this site produced a rotational level of 6.84 meV for the lowest transition, which is in excellent agreement with the lowest energy peak observed in the INS spectra for the MOF.[48] Further, there are only 12 of these sites available within a unit cell of the MOF, which explains why the peak at *ca.* 6.8 meV is saturated below 1.5 H_2 per formula unit loading.

The INS spectra show a peak at approximately 9.0 meV that gradually increases in intensity at higher loadings. This peak is typical for H_2 sorbing onto a single Cu^{2+} ion of the copper paddlewheel unit as observed in **rht**-MOF-1 (Fig. 4(a)),[25,52] **rht**-MOF-4a (Fig. 4(b)),[25] HKUST-1,[50] and PCN-12.[51] In the case of **rht**-MOF-7, the *ca.* 9.0 meV peak is associated with sorption onto the CuA ions, the Cu^{2+} ions that project into the cub-O_h cages in the MOF (Fig. 5(b)). This was indeed confirmed through two-dimensional quantum rotation calculations.[48] Unlike the environment of the CuB ions, the CuA ions are much farther apart from each other. Thus, as the H_2 molecule sorbs onto the CuA ions, it cannot interact with any other components of the MOF structure. This results in a relatively weaker interaction compared to sorption between two neighboring CuB ions. Note, the intensity of the 9.0 meV peak is nearly twice as high as that for the 6.8 meV peak at the highest loading measured (4 H_2 per formula unit). This is consistent with the expected relative saturation amounts about both types of Cu^{2+} ions as there are two CuA sites for every region between two adjacent CuB ions.

Additional peaks can be observed at approximately 11.0 and 13.5 meV in the INS spectra for **rht**-MOF-7, especially at low loadings. GCMC simulations and two-dimensional quantum rotation calculations provided clarification on the identity of these sites.[48] The center of the linker in the MOF can sorb up to three H_2 molecules, with each sorbate interacting with a N atom on the 1,3,5-triazine group (Fig. 5(c)). This suggests that the peak at about 11.0 meV could correspond to sorption onto the 1,3,5-triazine moieties since the intensity of this peak at the highest loading is about three times as high as that for the lowest energy peak in the spectra. This was convincingly supported by two-dimensional quantum rotation calculations, as such calculations for H_2 sorbed onto the 1,3,5-triazine groups yielded a $j = 0$ to $j = 1$ transition near 11 meV.

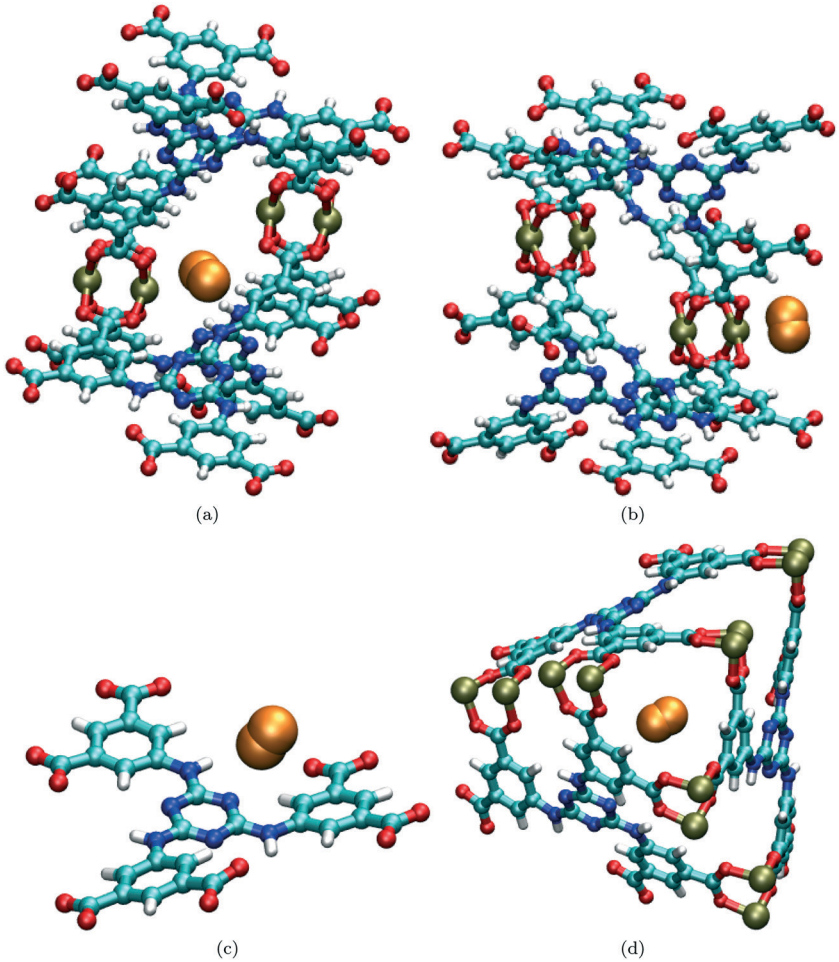

Fig. 5 Molecular illustration of a H_2 molecule (orange) sorbed at various sites in **rht**-MOF-7 as determined from the GCMC simulations performed in ref. 48: (a) between two CuB ions, (b) onto a single CuA ion, (c) onto the 1,3,5-triazine groups of the linkers, and (d) within the corner of the T-T_d cage. These sorption sites correspond to the peaks observed at approximately 6.8, 9.0, 11.0 and 13.5 meV, respectively, in the INS spectra for the MOF (Fig. 4(c)). Atom colors: C = cyan, H = white, N = blue, O = red, Cu = tan. These figures were reproduced from ref. 48 within the guidelines provided by the American Chemical Society. Copyright 2014 American Chemical Society.

GCMC simulations of H_2 sorption in **rht**-MOF-7 revealed that the H_2 molecules also occupy the corners of the T-T_d cages (Fig. 5(d)),[48] similar to what was observed for D_2 sorption in NOTT-112 through NPD (see section II.A).[13] Two-dimensional quantum rotation calculations for H_2 sorbed in this area generated rotational levels that are close to 13.5 meV for the two lowest $j = 0$ to $j = 1$ transitions.[48] Thus, the peak at *ca.* 13.5 meV in the INS spectra should correspond to H_2 sorbing within the corners of the T-T_d cages. This also makes sense from a loading perspective since up to four H_2 molecules can sorb within this region according to the GCMC simulations and the intensity of the 13.5 meV peak is approximately four times as high as that for the lowest energy peak.

Overall, INS studies of H_2 sorbed in **rht**-MOF-1, **rht**-MOF-4a, and **rht**-MOF-7 revealed that the Cu^{2+} ions of the copper paddlewheels are the principal binding sites for H_2 in these MOFs. This was exemplified by the fact that the spectra for all three MOFs contain a peak occurring at about 9.0 meV for all loadings measured. The presence of different functionalities in these **rht**-MOFs also gave rise to distinct features in the individual spectra. As demonstrated in the context of **rht**-MOF-1 (ref. 52) and **rht**-MOF-7 (ref. 48), the assignments of the peaks in the INS spectra can be verified through GCMC simulations and attendant quantum dynamics calculations.

III. Theoretical studies

A. Monte Carlo simulations

By far most of the elucidation of the binding sites in **rht**-MOFs have been made by way of Monte Carlo (MC) simulations, particularly within the grand canonical ensemble. Indeed, a number of GCMC simulation studies of gas sorption have been reported that yielded insights into the binding sites in these MOFs.[27,28,33,45,48,52,56–61] We note that there are other GCMC simulation studies performed on **rht**-MOFs, particularly by Snurr and co-workers,[14,23,24,29,30] but such works were more focused on showing the comparisons between experimental and theoretical observables.

In short, GCMC simulations involve the random trial movement of sorbate molecules within a simulation box

containing the MOF–sorbate system in which the chemical potential, volume, and temperature are kept fixed.[62] Gibbs ensemble Monte Carlo (GEMC) is another technique that can be used to perform simulations of gas sorption in MOFs as demonstrated by Babarao *et al.*[53] This method involves utilizing two simulation boxes, one for the MOF and another for the sorbates.[63] The volume of the sorbent is kept fixed, but that for the sorbate is allowed to vary at a fixed pressure. In addition, the total number of sorbates in a GEMC simulation is kept fixed, but the sorbates can swap from one box to another. In this section, we discuss the sorption sites that were observed through selected MC simulation studies on various **rht**-MOFs.

1. rht-MOF-1. Perhaps the earliest MC simulation study of gas sorption on an **rht**-MOF was performed by Babarao *et al.* in 2010.[53] In that work, the authors performed simulations of H_2 and CO_2 sorption in **rht**-MOF-1 using GEMC methods. They determined the favorable H_2 and CO_2 sorption sites in the MOF at different pressures. The CO_2/H_2 separation performance of the MOF was also investigated in that study.

As stated earlier (in section II.B.1), **rht**-MOF-1 is a cationic MOF that contains extra-framework nitrate counterions within the material. These NO_3^- ions are located within the cub-O_h cages in the solvated structure of the MOF. Molecular dynamics (MD) simulations revealed that these nitrate counterions migrate to the corners of the T-T_d cages in the dehydrated structure; these regions therefore represent the equilibrium locations of the NO_3^- ions in the solvent-free material. The authors in ref. 53 carried out GEMC simulations on **rht**-MOF-1 with the nitrate ions positioned in the corners of the T-T_d cages. Note, the aforementioned finding for the equilibrium locations of the NO_3^- ions in the dehydrated **rht**-MOF-1 was also reproduced from theoretical studies in our group.[52]

Babarao *et al.* evaluated the preferred H_2 sorption sites in **rht**-MOF-1 by plotting the density contours of H_2 sorbed in the MOF at 77 K and different pressures.[53] The density contour plots that they generated at 77 K and 10, 100, and 1000 kPa are shown in Fig. 6. At 10 kPa, it can be observed that the H_2 molecules mainly sorb onto the nitrate counterions that are located in the corners of the T-T_d cages. This suggests that the unbound NO_3^- ions are the most favorable sorption sites for H_2 in **rht**-MOF-1 since they are highly occupied at low loading.

At 100 kPa, the density contours reveal that the H_2 molecules occupy the regions intersecting the cub-O_h and T-O_h cages as well as the cub-O_h and T-T_d cages.[53] The H_2 molecules further populate these intersecting regions at 1000 kPa. Moreover, occupancy can be observed within the T-T_d cages at this pressure. Interestingly, the COM distributions of NO_3^- ions are similar across all three pressures, implying that the positions of these counterions do not change significantly upon H_2 sorption at 77 K and varying pressures.

Simulations of H_2 sorption in **rht**-MOF-1 were also carried out by our group previously using GCMC methods.[52] The three-dimensional histogram showing the most frequent sites of H_2 occupancy in the MOF at 77 K and a very low pressure (0.001 atm) is displayed in Fig. 7. It can be observed that the majority of H_2 molecules are sorbed onto the nitrate counterions within the corners of the T-T_d cages at this loading. This is consistent with what was discovered by Babarao *et al.* from their simulations in **rht**-MOF-1 at low pressure.[53] Indeed, these NO_3^- counterions represent the most favorable H_2 sorption sites in the MOF since they are charged particles that increase the electrostatic field within the framework. It appears that they are more preferred than any of the open-metal sites in the MOF. Furthermore, sorption onto these counterions correspond to the initial H_2 Q_{st} of the MOF as supported by our close reproduction of the experimental Q_{st} plot from GCMC simulations.[52]

Note, in our theoretical study on **rht**-MOF-1, we also observed sorption onto the Cu^{2+} ions of the $[Cu_2(O_2CR)_4]$ and $[Cu_3O(N_4CR)_3]$ units.[52] Such metal sites were captured in the simulations due to implementing many-body polarization interactions. After the NO_3^- counterions, the Cu^{2+} ions of the copper paddlewheels represent the next most favorable binding site, followed by the Cu^{2+} ions of the Cu_3O trimers. This is consistent with what was discerned through INS studies on the MOF (see section II.B.1).[25] These Cu^{2+} ion sites were not reproduced in the work of Babarao *et al.*,[53] presumably due to the lack of explicit polarization effects in their simulations. At higher loadings, sorption was also identified within the cub-O_h cages in the MOF.[52] The authors in ref. 53 also claimed to observe H_2 sorbing into these cages at higher pressures.

Babarao *et al.* also examined the CO_2 binding sites in **rht**-MOF-1 in their work.[53] The authors stated that the CO_2 sorption sites are similar to those shown in Fig. 6 for H_2 sorption. However, they observed that the locations of the NO_3^- ions are more dispersed due to the greater thermal motion at 298 K. In addition to plotting the density contours and three-dimensional histograms and inspecting the modeled structure for binding sites, the preferential sorption sites in a MOF can be monitored through analysis of the radial distribution function ($g(r)$). Here, the normalized particle number for a sorbate is plotted at varying distances from a reference atom (usually from the host). This was demonstrated in ref. 53, where the authors evaluated the $g(r)$ of CO_2 about the nitrate ions in **rht**-MOF-1.

Fig. 8 shows the $g(r)$ of CO_2 carbon atoms about the N atoms of the NO_3^- ions in **rht**-MOF-1 at 298 K and different pressures (10, 100, and 1000 kPa). At 10 kPa, a significant peak can be observed at approximately 3.3 Å. This peak indicates a considerable amount of CO_2 molecules sorbing onto the nitrate ions at low loading. Indeed, as in the case of H_2, a very strong interaction exists between the CO_2 molecules and the NO_3^- ions. Hence, these counterions represent favorable sorption sites for CO_2 in **rht**-MOF-1. It can be observed that the magnitude of the peak at *ca.* 3.3 Å decreases at higher pressures. This is because, in addition to the nitrate ions, the CO_2 molecules are sorbing onto other regions in the MOF structure at higher loadings, most notably, the regions intersecting the cub-O_h/T-O_h cages and cub-O_h/T-T_d cages; this results in a lower relative occupancy about such counterions. Note, our group also used $g(r)$ analysis to evaluate the favorable binding sites in **rht**-MOFs.[36,45,48,52,56,58,59,61]

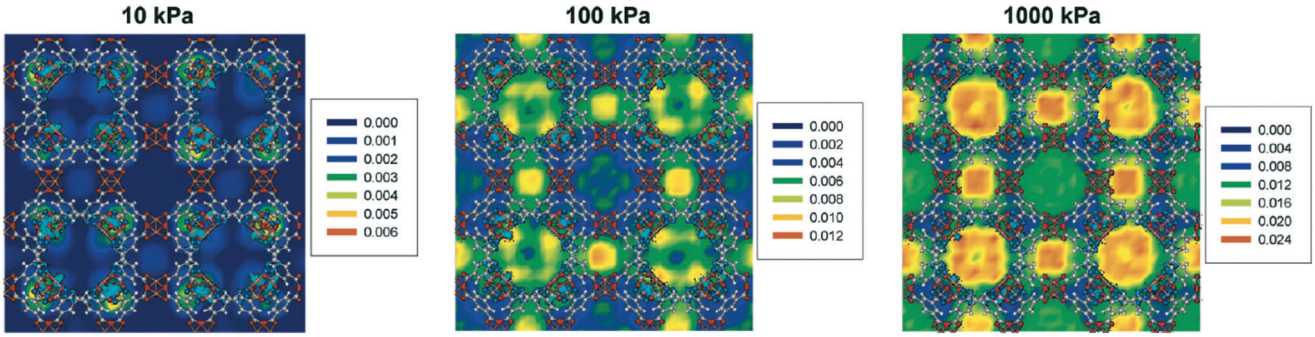

Fig. 6 Density contours of H_2 molecules in **rht**-MOF-1 at 77 K and 10 (left), 100 (middle), and 1000 kPa (right) based on the number of H_2 molecules per Å^3 according to the GEMC simulations performed in ref. 53. The COM distributions of NO_3^- counterions are depicted in cyan. Atom colors: C = gray, H = white, N = blue, O = red, Cu = peach. This figure was reproduced from ref. 53 within the guidelines provided by the American Chemical Society. Copyright 2010 American Chemical Society.

2. PCN-61. The first study that demonstrated the importance of explicit many-body polarization interactions on gas sorption in an **rht**-MOF was performed by our group in 2012, where H_2 sorption was theoretically investigated in PCN-61.[56] This **rht**-MOF consists of Cu^{2+} ions coordinated to 5,5′,5″-benzene-1,3,5-triyltris(1-ethynl-2-isophthalate) linkers (L3 and Fig. 2).[11,12] The linker of this MOF is relatively simple, which makes it an attractive candidate for baseline computational studies. PCN-61 has an estimated BET surface area of 3000 $m^2\ g^{-1}$ (Langmuir surface area is 3500 $m^2\ g^{-1}$), a pore volume of 1.36 $cm^3\ g^{-1}$, and a porosity of 77%. Experimental gas sorption measurements revealed that the MOF has a H_2 uptake of 2.25 wt% at 77 K/1 atm and a zero-loading Q_{st} value of 6.36 kJ mol^{-1}.[12] Additionally, PCN-61 exhibited an excess CO_2 uptake of about 3.15 mmol g^{-1} at 298 K/1 atm (ref. 15) and an initial CO_2 Q_{st} of 21–22 kJ mol^{-1}.[12,15]

In our work on PCN-61,[56] we showed that simulations using a polarizable H_2 potential[64] generated sorption isotherms and Q_{st} values that are in outstanding agreement with the corresponding experimental measurements for the MOF. On the other hand, simulations utilizing potentials that neglect this interaction[64,65] failed to reproduce experimental observables. Further, the inclusion of explicit many-body polarization effects was necessary to capture the sorption of H_2 onto the open-metal sites in the MOF.[56]

Simulations involving explicit many-body polarization interactions allow for the binding sites to be discerned through the distribution of the induced dipoles on the sorbate molecules. This was first demonstrated in the MC simulation studies carried out by Belof *et al.* on In-**soc**-MOF.[66] The normalized sorbate population is plotted as a function of the induced dipole magnitudes. The resulting dipole distribution for a sorbate in a MOF contain a number of different peaks, with each peak generally correlating to a region of occupancy in the material. In general, a peak that is found at high induced dipole magnitudes corresponds to sorption onto the

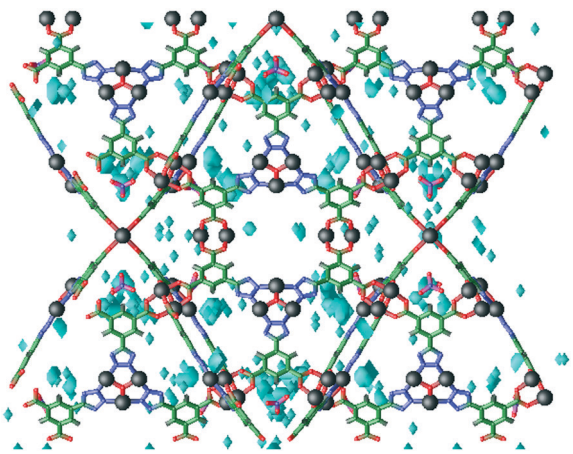

Fig. 7 Three-dimensional histogram showing the most frequent sites of occupancy (cyan) for H_2 molecules in **rht**-MOF-1 at 77 K and 0.001 atm according to the GCMC simulations performed in ref. 52. Atom colors: C = green, H = white, N = blue, O = red, Cu = black. This figure was reproduced from ref. 52 within the guidelines provided by the Royal Society of Chemistry. Copyright 2014 Royal Society of Chemistry.

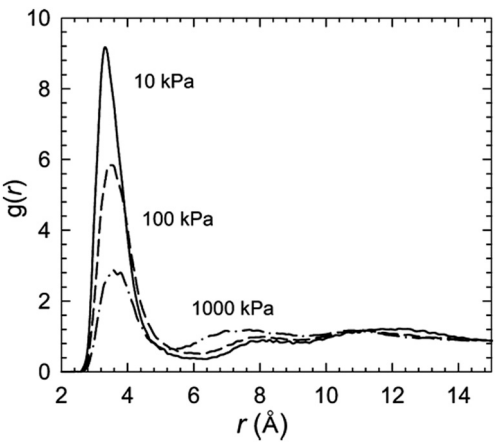

Fig. 8 Radial distribution function (g(r)) of CO_2 carbon atoms around the COM of the NO_3^- counterions in **rht**-MOF-1 at 298 K and 10 (solid), 100 (dashed), and 1000 kPa (solid and dotted) according to the GEMC simulations performed in ref. 53. This figure was reproduced from ref. 53 within the guidelines provided by the American Chemical Society. Copyright 2010 American Chemical Society.

most favorable binding sites in the MOF. This is because such sites induce high dipoles on the sorbate.

Fig. 9 shows the sorbate induced dipole magnitudes plotted against the normalized H_2 population in PCN-61 at 77 K and various pressures (0.02, 0.15, 0.30, 0.50, and 1.0 atm) as obtained from simulations using a polarizable H_2 potential in the MOF.[56] A broad peak can be observed from about 0.25–0.50 D, which is most notable at the lowest loading considered (0.02 atm). This peak corresponds to H_2 sorbing onto the exposed Cu^{2+} ions in the MOF as verified through examining the regions of sorbate occupancy for H_2 molecules with these induced dipole magnitudes. Specifically, these H_2 molecules were found to sorb onto the CuA ions as presented in Fig. 10(a). Indeed, the highly charged and polar Cu^{2+} ions of the copper paddlewheels induce rather high dipoles on the H_2 molecules, which have a permanent dipole moment of 0 D in bulk on average.

A second peak can be observed from approximately 0.05–0.10 D in the H_2 dipole distribution for PCN-61. Correlating this peak to regions of occupancy in the MOF revealed that H_2 molecules with these induced dipoles sorb into the corners of the T-T_d cages.[56] This area was also discovered as a sorption site in other neutral **rht**-MOFs, such as NOTT-112 (section II.A)[13] and **rht**-MOF-7 (section II.B.3).[48] Note, such induced dipole magnitudes are comparable to that for the permanent dipole on CO (0.122 D),[67] which has a normal boiling point of 82 K. An additional peak that increases in intensity at higher pressures can be observed from 0.0–0.05 D. This peak corresponds to H_2 molecules crowding into the more spacious regions of the MOF (*e.g.*, the center of the T-T_d and T-O_h cages).[56] As H_2 molecules are sorbed into such areas, the sorbates exhibit lower induced dipoles since they are nearly representative of "free" H_2.

3. Cu-TPBTM. The significance of many-body polarization interactions on gas sorption in MOFs with highly charged and polar sites was further demonstrated from GCMC simulation studies of H_2 sorption in another **rht**-MOF known as Cu-TPBTM.[58] This is a Cu^{2+}-based **rht**-MOF that was constructed using *N*,*N*′*N*″-tris(isophthalyl)-1,3,5-benzenetricarboxamide (L5 in Fig. 2) as the linker.[15] The BET/Langmuir surface area and pore volume for this MOF were measured to be 3160/3570 $m^2\ g^{-1}$ and 1.27 $cm^3\ g^{-1}$, respectively. In essence, the linker of Cu-TPBTM contains polar amide groups in place of the nonpolar alkyne groups observed in PCN-61. This contributes to a more polar structure overall, allowing this MOF to exhibit superior gas sorption performance relative to PCN-61. For instance, experimental studies have shown that Cu-TPBTM displays H_2 and CO_2 uptakes of 2.61 wt% and 5.29 mmol g^{-1} at 77 K/1 atm and 298 K/1 atm, respectively.[15,58] This quantity for the CO_2 uptake is only lower than that for **rht**-MOF-7 (ref. 19) and **rht**-MOF-9 (ref. 31) within the **rht**-MOF family under the same conditions. Further, the experimental initial H_2 and CO_2 Q_{st} values were determined to be 6.6 and 26.3 kJ mol^{-1}, respectively.[15,58]

Although Cu-TPBTM and PCN-61 are highly isostructural, differing only in the functionality located between the isophthalate groups and the central aromatic ring of the linker (as well as minor differences in the unit cell lengths, pore sizes, *etc.*), they exhibit distinct gas sorption mechanisms at low loading according to the GCMC simulations performed by our group.[58] As with PCN-61, we showed that implementing classical polarization was requisite for reproducing experimental observables and capturing the sorption of H_2 onto the open-metal sites in Cu-TPBTM. However, *ab initio* calculations revealed that Cu-TPBTM exhibits a different charge distribution about the copper paddlewheels compared to PCN-61; this had an effect on the initial binding sites in both MOFs.

Electronic structure calculations on different representational fragments of PCN-61 indicate that the CuA ions, the Cu^{2+} ions projecting into the cub-O_h cages in the MOF, display a greater partial positive charge relative to the CuB ions.[56] Analogous calculations on Cu-TPBTM revealed the opposite trend, where it was discovered that the CuB ions, the Cu^{2+} ions projecting into the T-T_d and T-O_h cages, exhibit the higher partial positive charge.[58] The CuA ions have a greater partial positive charge in PCN-61 probably due to the fact that they are located in a more favorable chemical environment in general by projecting into the cub-O_h cages. However, in Cu-TPBTM, it appears that the presence of the negatively charged amide O atom on the linker causes the partial positive charge of the CuB ions to increase through an inductive effect (and thereby decreasing its electron density) since the amide groups are proximal to such Cu^{2+} ions in the structure. This could explain why the partial positive charge is greater on the CuB ions compared to the CuA ions in this MOF.

As explained briefly for NOTT-112 in section II.A., the sorbate molecules are more attracted to the type of Cu^{2+} ion having the higher partial positive charge in **rht**-MOFs. Indeed, GCMC simulations of H_2 sorption in PCN-61 and Cu-TPBTM with the inclusion of explicit many-body polarization interactions revealed that the H_2 molecules sorbed initially onto the CuA ions in the former (Fig. 10(a)),[56] and onto the CuB ions

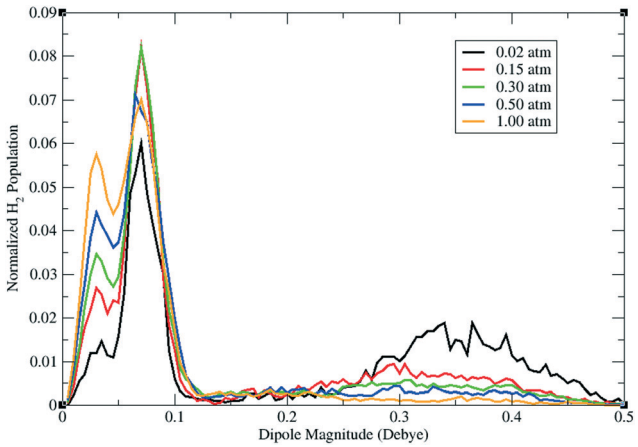

Fig. 9 Normalized distribution of the induced dipoles on H_2 molecules sorbed in PCN-61 at 77 K and various pressures (0.02 atm = black, 0.15 atm = red, 0.30 atm = green, 0.50 atm = blue, 1.00 atm = orange) according to GCMC simulations involving explicit many-body polarization performed in ref. 56. This figure was reproduced from ref. 56 within the guidelines provided by the American Chemical Society. Copyright 2012 American Chemical Society.

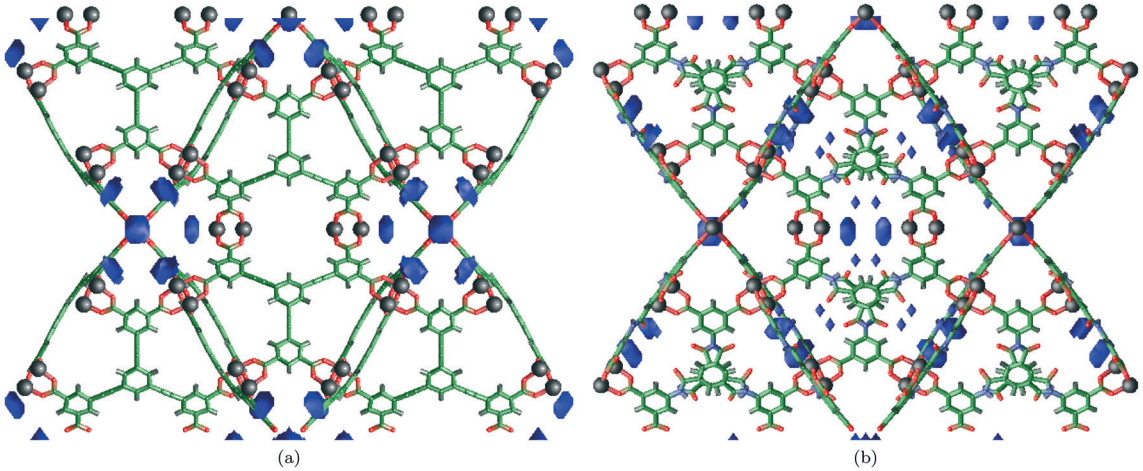

Fig. 10 Three-dimensional histogram showing the initial H_2 sorption sites (blue) in (a) PCN-61 and (b) Cu-TPBTM about the CuA and CuB ions, respectively, as determined from GCMC simulations involving explicit many-body polarization performed in ref. 56 and 58. Atom colors: C = green, H = white, N = blue, O = red, Cu = black. These figures were reproduced from ref. 58 within the guidelines provided by the American Chemical Society. Copyright 2013 American Chemical Society.

in the latter (Fig. 10(b)).[58] In other words, for the primary sorption site, the H_2 molecules bind onto the Cu^{2+} ions located ***inside*** the cub-O_h cages in PCN-61, whereas they sorb onto the Cu^{2+} ions located ***outside*** the cub-O_h cages in Cu-TPBTM. We note that sorption of H_2 was also observed within the corners of the T-T_d cages and onto the amide groups in Cu-TPBTM according to GCMC simulations.[58] Additionally, a similar phenomenon was observed in the case of CO_2 sorption in both of these **rht**-MOFs.[61]

4. rht-MOF-7. The first GCMC simulation study of gas sorption on **rht**-MOF-7 was performed by Zhang *et al.* in 2012.[57] In that work, the authors generated simulated CO_2, CH_4, and N_2 sorption isotherms in good agreement with the experimental measurements reported in ref. 19 using the potentials developed by the TraPPE force field.[68] The authors also investigated CO_2/N_2 and CO_2/CH_4 selectivity in the MOF and concluded that the material could be promising for separating CO_2 from flue gas and natural gas.[57] To obtain structural information on CO_2 sorbed in **rht**-MOF-7, Zhang *et al.* plotted the density distribution profiles between the CO_2 molecules and the COM of the MOF at 298 K and 10 and 100 kPa; the resulting plots are shown in Fig. 11. Two noticeable peaks can be observed at approximately 9.6 and 15.2 Å. The authors in ref. 57 attributed these two peaks to CO_2 molecules sorbing onto the exposed Cu^{2+} ions and Lewis basic sites. The intensity of the peak at *ca.* 15.2 Å decreases substantially at the higher pressure, which could be due to CO_2 sorbing into the intersecting regions between two cages as well as the aforementioned sites.

GCMC simulations of gas sorption were also carried out in **rht**-MOF-7 by our group in 2014, where the CO_2 and H_2 sorption mechanism and binding sites in the MOF were investigated.[48] It was shown that the simulated CO_2 and H_2 sorption isotherms and Q_{st} values were in close agreement with the experimental measurements reported by Eddaoudi and co-workers.[20] These simulations were executed using polarizable potentials for the respective sorbates.[64,69] The inclusion of explicit many-body polarization interactions in simulation allowed for a significant quantity of CO_2 and H_2 molecules to sorb onto the open-metal sites in the MOF at low loading.[48]

A number of distinct CO_2 binding sites were observed in **rht**-MOF-7 from the simulations performed by our group.[48] The most favorable of these corresponds to the sorption of CO_2 between two neighboring CuB ions, where each oxygen atom of the sorbate interacts with a single Cu^{2+} ion of adjacent copper paddlewheels (Fig. 12(a)). This sorption site is actually an example of a single-molecule trap for CO_2, which has been similarly observed in other MOFs.[70,71] The small and angular nature of the L7 linkers permit two neighboring $[Cu_2(O_2CR)_4]$ clusters to be in proximity to each other, thus allowing this sorption site to exist in the material. Further, this binding site corresponds to the initial CO_2 Q_{st} value for the MOF (*ca.* 45 kJ mol^{-1})[20] as

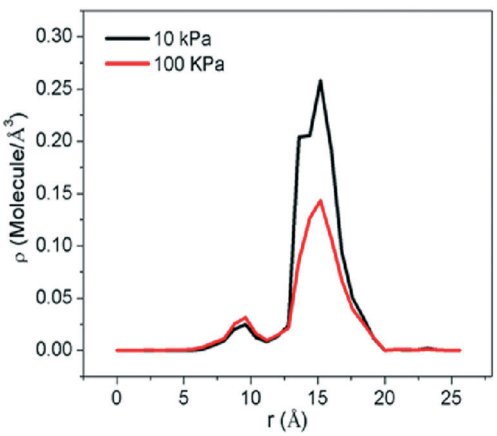

Fig. 11 Density distribution profiles between CO_2 and the COM of **rht**-MOF-7 at 298 K and 10 (black) and 100 kPa (red) according to the GCMC simulations performed in ref. 57. This figure was reproduced from ref. 57 within the guidelines provided by the American Chemical Society. Copyright 2012 American Chemical Society.

validated through our classical GCMC simulations involving explicit polarization.[48] Indeed, as demonstrated in the context of **rht**-MOF-7, the current smallest member of the **rht**-MOF family, tuning the pore sizes in MOFs can lead to optimal interactions between the sorbate molecules and the framework.

The next most preferrential sorption sites for CO_2 in **rht**-MOF-7 are the CuA ions.[48] An illustration of a CO_2 molecule sorbing onto this site is shown in Fig. 12(b). Unlike what was observed about the CuB ions, a CO_2 molecule can only sorb onto a single CuA ion since such Cu^{2+} ions are positioned farther apart from each other as a result of being located in the cub-O_h cages. The interaction for sorption onto a CuA ion is weaker than that for binding between two adjacent CuB ions. GCMC simulations revealed that the corners of the T-T_d and T-O_h cages and the 1,3,5-triazine groups are also sites of occupancy for the CO_2 molecules in the MOF, especially at higher loadings. These CO_2 sorption sites were also discovered in the simulation studies performed by Jiang's group in ref. 60, which was the third paper that reported theoretical gas sorption results in **rht**-MOF-7. Note, the preferred H_2 binding sites in the MOF were also identified from our simulations;[48] these sites are discussed in section II.B.3 and shown in Fig. 5.

5. NTU-105. NTU-105 (ref. 27) (also known as NOTT-122a (ref. 28) or NU-125 (ref. 29)) is another **rht**-MOF that contains N-rich centers in the structure. This MOF was synthesized by combining Cu^{2+} ions with 5,5′,5″-(4,4′,4″-(benzene-1,3,5-triyl)tris(1*H*-1,2,3-triazole-4,1-diyl))triisophthalate linkers (L8 in Fig. 2). NTU-105 was synthesized by three different groups in early 2013,[27–29] with all three groups reporting their own distinct gas sorption measurements and crystal structure of the MOF. Overall, the three experimental groups have shown that this MOF displays remarkable CO_2 sorption performance, which could be attributed to the presence of open-metal sites and 1,2,3-triazole groups in the structure.

The measured CO_2 uptakes for the MOF by the three groups at 298 K/1 atm are similar to each other (*ca.* 4.2, 4.6, and 4.0 mmol g^{-1} in ref. 27–29, respectively). When comparing to other MOFs within the **rht**-MOF platform, only **rht**-MOF-7,[19] **rht**-MOF-9,[31,33] and Cu-TPBTM[15] have higher experimental CO_2 uptakes under the same conditions to the best of our knowledge. In addition, according to the empirical fitting by Wang *et al.*,[27] NTU-105 exhibits an initial CO_2 Q_{st} of about 36 kJ mol^{-1}, which is third to only **rht**-MOF-7 (ref. 19 and 20) and **rht**-MOF-9 (ref. 31) in the **rht**-MOF family. The same authors demonstrated that the MOF has a H_2 uptake of 2.75 wt% at 77 K/1 atm and a zero-loading Q_{st} value of roughly 6.6 kJ mol^{-1}.[27] This value for the H_2 uptake is among the highest of reported **rht**-MOFs at the same state point.[27,34] NTU-105 was also shown to be one of the top sorbents for CH_4 storage.[29,72]

The three experimental references for NTU-105 also list the results from GCMC simulations of gas sorption in the MOF.[27–29] All three groups reported simulated gas sorption isotherms in decent agreement with their experimental measurements using nonpolarizable potentials.[68,73] Attempts at elucidating the favorable binding sites for CO_2 in NTU-105 were made by Wang *et al.*[27] and Yan *et al.*[28] The former investigated the interactions between the CO_2 molecules and the MOF by analyzing the g(r) of these sorbates around different framework atoms.[27] Fig. 13 shows the g(r) of CO_2 carbon atoms about the Cu^{2+} ions of the copper paddlewheels and the various N atoms of the 1,2,3-triazole groups of the linker in NTU-105 at 298 K and three different pressures (1, 10, and 100 kPa). The three distinct N atoms are denoted N1, N2, and N3, where N1 represents the N atom connected to the isophthalate group and N3 is the N atom that is closest to the central aromatic ring. Note, unlike what was implemented in other GCMC simulation studies on **rht**-MOFs,[28,33,45,48,52,56,58–61] the simulations in ref. 27 treated all Cu^{2+} ions as chemically equivalent.

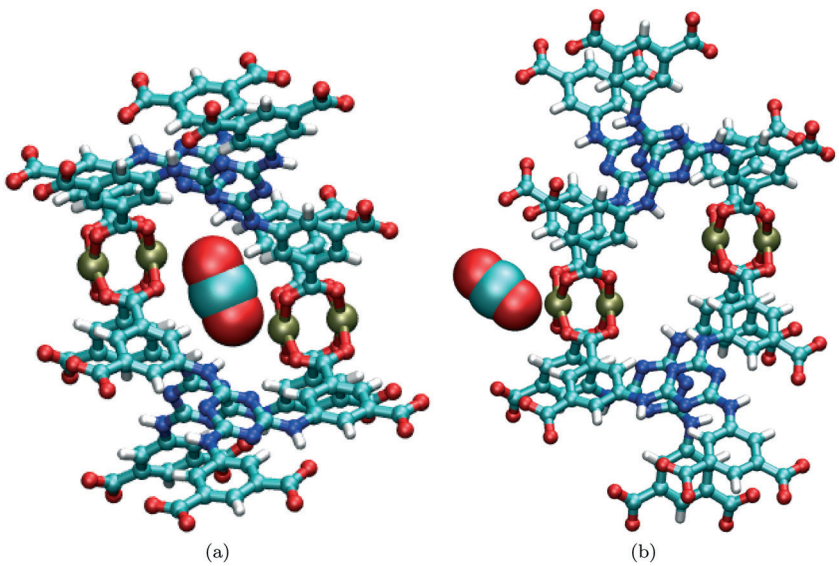

Fig. 12 Molecular illustration of a CO_2 molecule sorbed (a) between two CuB ions and (b) onto a single CuA ion in **rht**-MOF-7 as determined from the GCMC simulations performed in ref. 48. Atom colors: C = cyan, H = white, N = blue, O = red, Cu = tan. These figures were reproduced from ref. 48 within the guidelines provided by the American Chemical Society. Copyright 2014 American Chemical Society.

The g(*r*) of CO_2 carbon atoms about the Cu^{2+} ions at all three pressures reveal a modest nearest-neighbor peak ranging from *ca.* 3.2–3.6 Å. This suggests that there are some CO_2 molecules sorbing onto the open-metal sites in NTU-105 within the simulations. The aforementioned range for the Cu^{2+}–$C(CO_2)$ interaction is comparable to that observed in HKUST-1 through NPD studies.[74] The significant peak spanning from approximately 5.2–6.8 Å (maximum at 6.0 Å) in the g(*r*) around the metals probably corresponds to CO_2 localizing in the corners of the T-T_d cages. Additionally, it can be deduced that the CO_2 molecules display strong affinity toward the N1 atoms as exemplified by the large peak ranging from *ca.* 4.4–6.0 Å in the g(*r*) about such atoms across all pressures. The CO_2 molecules also exhibit favorability toward the N2 and N3 atoms since the g(*r*) of sorbates about these N atoms reveal a nearest-neighbor peak occurring at short distances.

Yan *et al.* discovered a number of different CO_2 sorption sites in NTU-105 from their GCMC simulations by inspecting the modeled structure at 298 K and various pressures.[28] At 10 kPa, the authors identified that the CO_2 molecules initially sorb onto the CuA ions in their simulations, which they denoted site I (Fig. 14(a)). This site is analogous to what is depicted in Fig. 12(b) for **rht**-MOF-7. At the same pressure, two additional CO_2 sorption sites were observed, which the authors referred to as sites II and III (Fig. 14(b)). Site II corresponds to the sorption of CO_2 in the center of the triangular-shaped window formed by three isophthalate moieties and three $[Cu_2(O_2CR)_4]$ clusters in the T-T_d cage. This site is essentially located in the corner of the T-T_d cage, which has been observed as a favorable binding site for the sorbate in other **rht**-MOFs through MC simulations.[48,53,59,61] Site III is located within the region formed by the peripheral arms from three different L8 linkers in the T-T_d cage, where the CO_2 is proximal to the N1 atom. This site is consistent with what was discerned in the g(*r*) of CO_2 molecules about the N1 atoms in the GCMC simulation studies executed by Wang *et al.*[27]

At a higher pressure (50 kPa), the authors in ref. 28 observed that the CO_2 molecules crowd into the spacious region of the T-T_d cage (Fig. 14(c)) and the small cavity surrounded by four L8 linkers connecting the T-T_d and T-O_h cages (Fig. 14(d)). They also identified a significant amount of CO_2 molecules sorbing in the cub-O_h cages at this pressure. Further, at pressures of 50 and 100 kPa, their simulations revealed a chain of CO_2 molecules forming through the Cu^{2+}–CO_2, 1,2,3-triazole–CO_2, and CO_2–CO_2 interactions in the MOF (Fig. 15). Overall, the results from GCMC simulations performed by Wang *et al.*[27] and Yan *et al.*[28] confirmed that the presence of open-metal sites and polar 1,2,3-triazole groups in NTU-105 contributes to high CO_2 uptake in the material.

B. Electronic structure calculations

In contrast to MC simulations, very few studies utilized electronic structure methods (*e.g.*, *ab initio* and density functional theory (DFT)) to investigate the binding sites in **rht**-MOFs. This is likely because of the computational expense involved with implementing such quantum mechanical calculations on these MOFs. For example, periodic DFT calculations for a sorbate molecule localized in an **rht**-MOF are in fact computationally prohibitive due to the very large size of the unit cells of these materials. Thus, it is much more feasible to determine the sorption sites in these MOFs through classical MC simulations. However, electronic structure calculations can be used to assess the binding strength for a guest molecule sorbing about certain components or functionalities within the **rht**-MOF structure. These calculations typically involve optimizing the position of a sorbate molecule localized about a properly truncated cluster taken from the unit cell of the MOF and subsequently evaluating the binding energy. The magnitude of the calculated binding energy can provide indication on whether the sorption site is favorable in the MOF. To the best of our knowledge, we only know of electronic structure calculations of the sorbent–sorbate interaction performed in two studies for **rht**-MOFs: **rht**-MOF-9 in ref. 33 and **rht**-MOF-1 and **rht**-MOF-pyr in ref. 36.

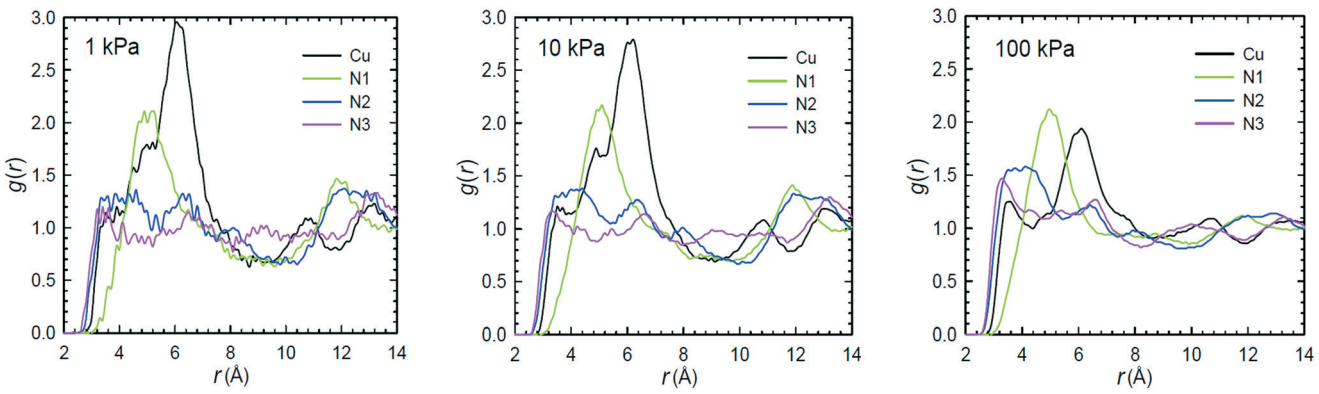

Fig. 13 Radial distribution function (g(*r*)) of CO_2 carbon atoms around the Cu^{2+} ions (black) and various N atoms on the 1,2,3-triazole group of the linker (N1 = green, N2 = blue, N3 = magenta) in NTU-105 at 298 K and 1 (left), 10 (middle), and 100 kPa (right) according to the GCMC simulations performed in ref. 27. This figure was reproduced from ref. 27 within the guidelines provided by the Nature Publishing Group. Copyright 2013 Nature Publishing Group.

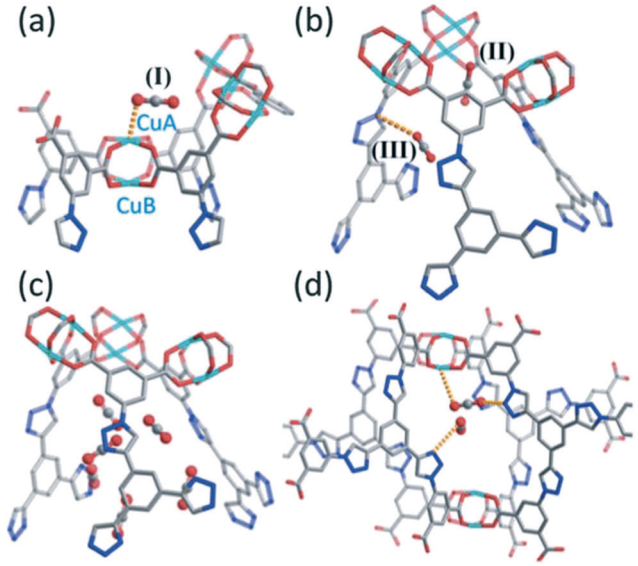

Fig. 14 Molecular illustration of the CO_2 sorption sites in NTU-105 at 298 K and ((a) and (b)) 10 kPa and ((c) and (d)) 50 kPa as determined from the GCMC simulations performed in ref. 28: (a) onto a single CuA ion (site I), (b) at sites II and III (see text in section III.A.5), (c) within the T-T_d cages, and (d) within the small cavity created by four L8 linkers connecting the T-T_d and T-O_h cages. Atom colors: C = gray, N = blue, O = red, Cu = cyan. This figure was reproduced from ref. 28 within the guidelines provided by the Royal Society of Chemistry. Copyright 2013 Royal Society of Chemistry.

1. rht-MOF-9. **rht**-MOF-9 (ref. 31) (also known as Cu-TDPAH (ref. 33)) is a MOF consisting of Cu^{2+} ions coordinated to 2,5,8-tris(3,5-dicarboxyphenylamino)-1,3,4,6,7,9,9b–heptaazaphenalene linkers (L9 in Fig. 2). The linker of this MOF is composed of a N-rich *s*-heptazine center connected to secondary amine groups, which in turn are bonded to isophthalate moieties. **rht**-MOF-9 represented the first example of an **rht**-MOF that contains a polycyclic central core in the linker. As with **rht**-MOF-7, this MOF was synthesized by two different groups,[31,33] with both groups publishing their own experimental gas sorption measurements and crystal structure data on the MOF. The CO_2 sorption isotherms measured at 298 K for **rht**-MOF-9 by the two groups were in fact comparable to each other. Moreover, Luebke *et al.* have shown that this MOF is capable of sorbing 2.72 wt% of H_2 at 77 K/1 bar and has an initial Q_{st} of 6.9 kJ mol^{-1}.[31] Liu *et al.* demonstrated that **rht**-MOF-9 exhibits high selectivity for CO_2 and C_2 hydrocarbons (C_2H_2, C_2H_4, C_2H_6) over CH_4.[33]

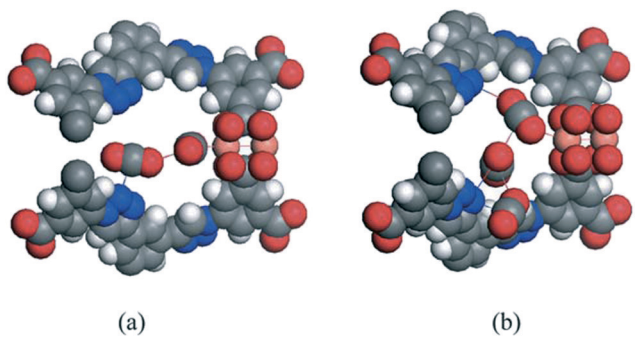

Fig. 15 Molecular illustration of the preferrential CO_2 sorption sites in NTU-105 at 298 K and (a) 50 kPa and (b) 100 kPa as determined from the GCMC simulations performed in ref. 28. Atom colors: C = gray, H = white, N = blue, O = red, Cu = peach. This figure was reproduced from ref. 28 within the guidelines provided by the Royal Society of Chemistry. Copyright 2013 Royal Society of Chemistry.

The authors in ref. 33 carried out GCMC simulations and DFT calculations in order to gain information on the CO_2 sorption sites in **rht**-MOF-9. Their GCMC simulations revealed that the CO_2 molecules prefer to sorb onto the Cu^{2+} ions of the copper paddlewheels and the secondary amine groups on the linker. In order to examine the role of the *s*-heptazine groups toward CO_2 sorption, Liu *et al.* carried out DFT calculations of a CO_2 molecule interacting with the secondary amine group on a truncated organic linker of the MOF and two other hypothetical variants of the linker in which the N content of the *s*-heptazine ring decreased sequentially. The calculations were performed at the 6-311++G(d,p)/B3LYP level of theory using the Gaussian09 package.[75] The optimized distances between the CO_2 oxygen atom and H atom of the secondary amine group as well as the calculated binding energies for the CO_2–HNR_2 interaction for all three model compounds are shown in Fig. 16.

Geometry optimizations revealed that the interaction distance between the CO_2 oxygen atom and the secondary amine H atom decreases with increasing number of N atoms on the polycylic aromatic ring. The binding energy associated with the CO_2–HNR_2 interaction for the truncated linker of **rht**-MOF-9 was calculated to be −10.3 kJ mol^{-1}, while those for the other two linkers are notably lower (both at −4.07 kJ mol^{-1}), indicating weaker guest–host interactions.[33] It is clear from these comparisons that the electronegative O atoms of the CO_2 molecule prefer to bind to the electropositive H atoms of the secondary amine group on the linker. However, the authors in ref. 33 attributed the stronger CO_2 affinity for the truncated linker of **rht**-MOF-9 to the greater density of N atoms on the polycylic aromatic ring, namely a synergistic effect with the N atoms that are proximal to the CO_2–HNR_2 interaction. Indeed, as the CO_2 molecule sorbs onto a secondary amine group of the L9 linker in the MOF, the positively charged C atom of the sorbate can also interact with the negatively charged N atom of the *s*-heptazine group that is nearby. We note that the richness of N atoms in **rht**-MOFs does not always lead to an increase in CO_2 sorption affinity as explained in the next section.

2. rht-MOF-1 and rht-MOF-pyr. In 2015, an isostructural analogue of **rht**-MOF-1 was constructed by substituting 5-tetrazolylisophthalate (L1 in Fig. 2) with 5-(1*H*-pyrazol-4-yl)isophthalate (L2 in Fig. 2).[35,36] This MOF, referred to as **rht**-MOF-pyr (or MPAF-1),[61] consists of pyrazole groups in place of the tetrazole groups observed in **rht**-MOF-1. Alternatively, the carbon-coordinated N atoms of the five-membered rings in **rht**-MOF-1 are substituted with CH groups in **rht**-MOF-pyr. Otherwise, both **rht**-MOFs contain the same structural features (*i.e.*, copper paddlewheels and Cu_3O trimers).

The BET surface area for the as-synthesized **rht**-MOF-pyr was measured to be 2133 $m^2\ g^{-1}$.[35]

Despite being highly isostructural to **rht**-MOF-1, **rht**-MOF-pyr was shown to display a much greater stability in moisture, water, steam, and acid.[35] Indeed, this MOF retained its crystallinity after being exposed to ambient air with a relative humidity (RH) of *ca.* 70% for a week, water for 15 days at room temperature, steam (100% RH at 100 °C) for 6 hours, and aqueous HCl solution with a pH of 2.5 for two weeks at 298 K. The BET surface area of **rht**-MOF-pyr did not change significantly after being subjected to the aforementioned conditions. Many other **rht**-MOFs do not display the same type of stability as they lose their crystallinity after prolonged exposure to air.[31,35] According to the electronic structure calculations performed by our group, the improved stability for **rht**-MOF-pyr relative to **rht**-MOF-1 can be attributed to the increase in electron density of the N atoms that are coordinated to the Cu^{2+} ions of the Cu_3O trimers, which resulted in stronger bonds with such Cu^{2+} ions.[35] This in turn lead to an increase in the stability about the $[Cu_2(O_2CR)_4]$ clusters. Note, an analogue containing 1,2,3-triazole groups was also synthesized in ref. 35 and shown to exhibit water and chemical stability.

rht-MOF-pyr was shown to display higher atmospheric CO_2 uptake than **rht**-MOF-1 at 273 and 298 K according to experimental measurements.[36] The former also exhibited a greater CO_2/CH_4 selectivity at 298 K/1 atm on the basis of ideal adsorbed solution theory (IAST) calculations.[76] These results seem counterintuitive as it was expected that **rht**-MOF-1 would display higher CO_2 uptake and selectivity due to possessing more N atoms on the framework. However, as demonstrated from GCMC simulations and DFT calculations carried out by our group, the local electric field of the $[Cu_3O(N_{4-x}(CH)_xCR)_3]$ (x = 0 or 2) units in the two MOFs played a more dominant role toward CO_2 sorption than the number of exposed N atoms on the linkers.[36]

GCMC simulations of CO_2 sorption in **rht**-MOF-1 and **rht**-MOF-pyr identified the NO_3^- counterions, the Cu^{2+} ions of the copper paddlewheels, and the Cu^{2+} ions of the Cu_3O trimers as favorable binding sites for the sorbate in both MOFs.[36] This is consistent with what was observed for H_2 sorption in **rht**-MOF-1 through related studies.[52] Since the main difference in the CO_2 uptakes among the two MOFs was expected to be due to the interaction between the CO_2 molecules and the Cu_3O trimers, additional calculations about such units were implemented, one of which included DFT calculations for a single CO_2 molecule positioned about the $[Cu_3O(N_{4-x}(CH)_xCR)_3]$ (x = 0 or 2) clusters for both **rht**-MOFs.[36] Such electronic structure calculations were performed to investigate the significance of substituting tetrazole with pyrazole on CO_2 sorption and to assess the difference in the binding energies about these MBBs.

The DFT calculations executed in ref. 36 utilized a truncated hexatopic building unit for both **rht**-MOFs, where all carboxylate groups of the L1 and L2 linkers were replaced with optimized H atoms. The CO_2 molecule was optimized to an energetically favorable position within both model compounds using the 6-31G* basis set for all C, H, N, and O atoms, the LANL2DZ effective core potential basis set[77] for the Cu^{2+} ions, and the B3LYP functional.[78,79] These calculations were performed with the NWChem *ab initio* software.[80] The optimized positions for a CO_2 molecule about a Cu^{2+} ion of the truncated hexatopic building unit for **rht**-MOF-1 and **rht**-MOF-pyr are shown in Fig. 17. The calculations revealed nearly equivalent distances for the Cu^{2+}–$O(CO_2)$ interaction, but notable differences in the orientation of the CO_2 molecule about these units.

It was observed that as the oxygen atom of the CO_2 molecule binds onto the Cu^{2+} ion of the Cu_3O trimer in **rht**-MOF-pyr, it can also interact with the nearby positively charged H atoms of the pyrazole groups simultaneously (Fig. 17(b)).[36] This synchronized binding keeps the sorbate molecule in-plane with respect to the $[Cu_3O(N_2(CH)_2CR)_3]$ trimers, resulting in a favorable interaction. In contrast, as the CO_2 oxygen atom sorbs onto the Cu^{2+} ion of the trimer in **rht**-MOF-1, it is repelled by the negatively charged N atoms of the tetrazole groups. In order to minimize N–O interactions, the CO_2 molecule orients at an angle and tilts out-of-plane with respect to the $[Cu_3O(N_4CR)_3]$ trimers, leading to a less favorable interaction (Fig. 17(a)). The magnitude of the calculated binding energy for the interaction between CO_2 and the Cu^{2+} ion of the truncated hexatopic

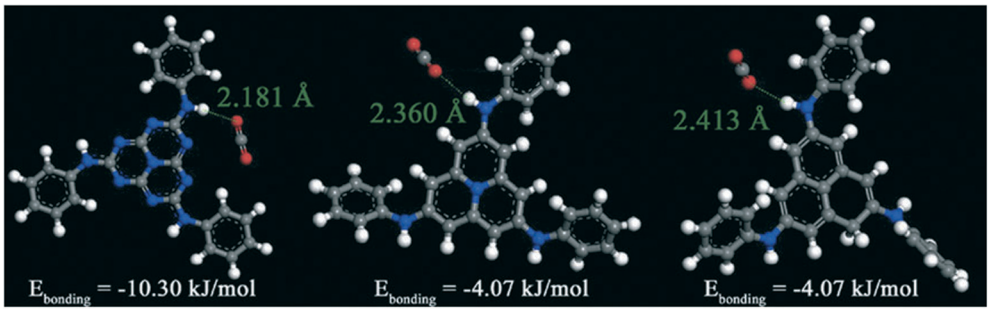

Fig. 16 Optimized position of a CO_2 molecule about the secondary amine groups within the truncated linker in **rht**-MOF-9 as well as different analogues of the *s*-heptazine unit as determined from the DFT calculations performed in ref. 33. The distances between the CO_2 oxygen atom and the H atom of the secondary amine group are shown along with the calculated binding energies. Atom colors: C = gray, H = white, N = blue, O = red. This figure was reproduced from ref. 33 within the guidelines provided by the Royal Society of Chemistry. Copyright 2014 Royal Society of Chemistry.

building unit was indeed greater for **rht**-MOF-pyr relative to **rht**-MOF-1 (−22.6 *vs.* −21.3 kJ mol^{-1}).

IV. Conclusion

The important experimental and theoretical studies that have yielded detailed insights into the gas sorption sites in MOFs belonging to the popular **rht**-MOF platform were discussed in this highlight. NPD experiments can perhaps provide the most definitive information on the sorption sites in these MOFs as demonstrated by Yan *et al.* on NOTT-112.[13] INS studies can give hints on the locations of the sorption sites in **rht**-MOFs based on the transition energies and intensities of the peaks observed in the spectra.[25,48] The assignments of the peaks within the INS spectra are usually tentative, but can be confirmed through calculation of the quantum dynamics within an accurate potential energy surface.[47]

MC simulations, especially those within the grand canonical ensemble, are probably the most convenient theoretical methods used to investigate the binding sites in **rht**-MOFs. The sorption sites can be determined through examining the modeled structure at various loadings. Plotting the density contours, three-dimensional histograms, g(r), induced dipole distributions, and density distribution profiles from the MC simulations have also been implemented to evaluate the binding sites in **rht**-MOFs. It is important to note that the accuracy of such classical simulations to predict the binding sites in these materials is typically dependent on the potential energy function utilized for the MOF and sorbate. Although less commonly employed, electronic structure calculations can reveal information on the orientation and binding energies for a sorbate localized about certain components or functionalities in **rht**-MOFs, as done previously for **rht**-MOF-9 in ref. 33 and **rht**-MOF-1 and **rht**-MOF-pyr in ref. 36.

We note that this paper discussed numerous studies that elucidated the H_2 and CO_2 sorption mechanisms and binding sites in **rht**-MOFs. To the best of our knowledge, the sorption sites for other guest molecules (*e.g.*, CH_4, N_2, C_2 hydrocarbons) in these MOFs have not been thoroughly explored, even though experimental gas sorption measurements were performed with such sorbates.[12,19,29,30,33] Nevertheless, it is likely that the binding sites for these gases in **rht**-MOFs are analogous to those described herein for H_2 and CO_2. Indeed, both of these sorbates occupied very similar sites in the structure for a particular **rht**-MOF.

On the basis of the studies summarized in this paper, it can be concluded that the most favorable sorbate binding sites in all neutral **rht**-MOFs are the exposed M^{2+} ions of the $[M_2(O_2CR)_4]$ clusters. The results from the NPD studies presented in ref. 13 clearly demonstrated that the M^{2+} ions that make up the metal paddlewheels in **rht**-MOFs are chemically distinct, and therefore exhibit different binding affinities toward the sorbates. This finding has been supported through GCMC simulations of gas sorption in various **rht**-MOFs.[28,45,52,56,58–61] The corners of the T-T_d cages have also been discovered as preferential sorption sites in these MOFs. In addition, if polar functional groups, such as amide,[15] secondary amine,[19,20,31,33] 1,3,5-triazine,[19,20] or 1,2,3-triazole[27–29] are present on the organic linkers, the sorbate molecules can interact with these moieties as well, generally leading to an increase in gas uptake at low pressures. In a cationic **rht**-MOF containing extra-framework counterions, such **rht**-MOF-1, the counterions represent the most favorable sorption sites for the guest molecules in these MOFs.[36,52,53] The M^{2+} ions that are part of the M_3O trimers are also preferred binding

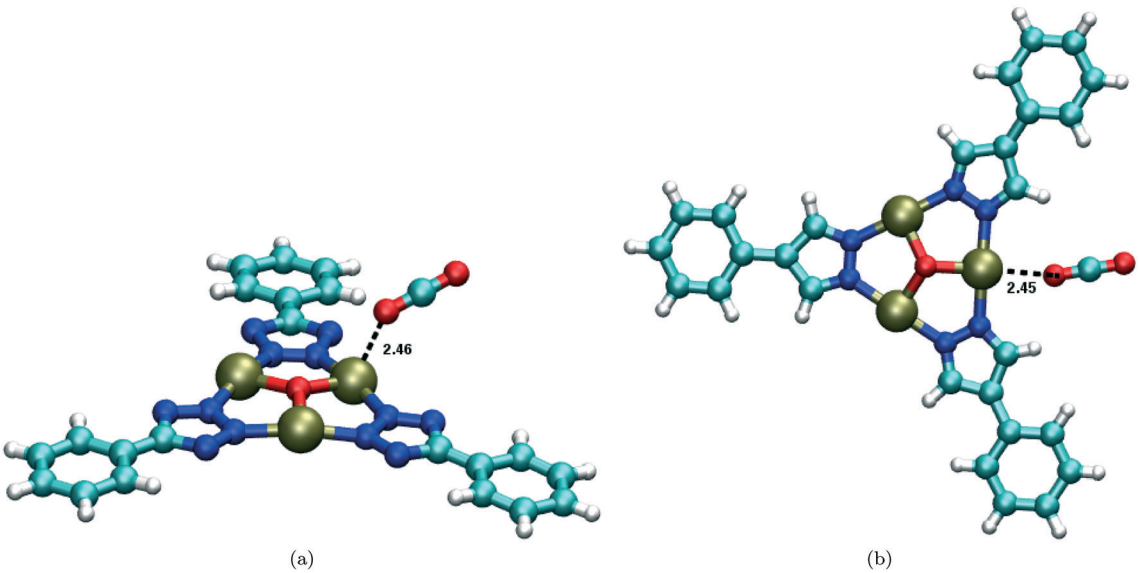

Fig. 17 Optimized position of a CO_2 molecule about the Cu_3O trimer within the truncated hexatopic building unit in (a) **rht**-MOF-1 and (b) **rht**-MOF-pyr as determined from the DFT calculations performed in ref. 36. The distances (in Å) between the Cu^{2+} ion and the closest O atom of the CO_2 molecule are also shown. Atom colors: C = cyan, H = white, N = blue, O = red, Cu = tan. These figures were reproduced from ref. 36 within the guidelines provided by the Royal Society of Chemistry. Copyright 2015 Royal Society of Chemistry.

sites in **rht**-MOFs possessing such clusters (*e.g.*, **rht**-MOF-1 and **rht**-MOF-pyr).[36,52] At higher loadings, sorption can be observed within the spacious regions of the three distinct cages of the **rht**-MOF structure.

The experimental and theoretical probing techniques described herein can provide significant understanding of the gas sorption mechanisms and binding sites in **rht**-MOFs and other types of MOFs in general. The results from such studies can help guide scientists and engineers to gain new perspectives into creating novel porous materials with improved gas uptake and adsorption enthalpy. After all, an ultimate goal in this energy economy is to synthesize innovative structures that can target certain environmental applications, such as addressing the challenging Department of Energy (DOE) targets for on-board H_2 and CH_4 storage[81,82] and effectively capturing CO_2 from post-combustion effluents or directly from the atmosphere to mitigate the global warming phenomenon.[83]

Conflicts of interest

There are no conflicts of interest to declare.

Acknowledgements

The authors acknowledge the National Science Foundation (Award No. DMR-1607989), including support from the Major Research Instrumentation Program (Award No. CHE-1531590). B. S. also acknowledges support from an American Chemical Society Petroleum Research Fund grant (ACS PRF 56673-ND6).

References

1 S. L. James, *Chem. Soc. Rev.*, 2003, **32**, 276–288.
2 M. P. Suh, H. J. Park, T. K. Prasad and D.-W. Lim, *Chem. Rev.*, 2012, **112**, 782–835.
3 T. A. Makal, J.-R. Li, W. Lu and H.-C. Zhou, *Chem. Soc. Rev.*, 2012, **41**, 7761–7779.
4 K. Sumida, D. L. Rogow, J. A. Mason, T. M. McDonald, E. D. Bloch, Z. R. Herm, T.-H. Bae and J. R. Long, *Chem. Rev.*, 2012, **112**, 724–781.
5 M. Eddaoudi and J. F. Eubank, in *Metal–Organic Frameworks: Design and Application*, ed. L. R. MacGillivray, John Wiley & Sons, Inc., Hoboken, NJ, 2010, pp. 37–89.
6 J. J. Perry IV, J. A. Perman and M. J. Zaworotko, *Chem. Soc. Rev.*, 2009, **38**, 1400–1417.
7 F. Nouar, J. F. Eubank, T. Bousquet, L. Wojtas, M. J. Zaworotko and M. Eddaoudi, *J. Am. Chem. Soc.*, 2008, **130**, 1833–1835.
8 Y. Zou, M. Park, S. Hong and M. S. Lah, *Chem. Commun.*, 2008, 2340–2342.
9 Y. Yan, X. Lin, S. Yang, A. J. Blake, A. Dailly, N. R. Champness, P. Hubberstey and M. Schröder, *Chem. Commun.*, 2009, 1025–1027.
10 S. Hong, M. Oh, M. Park, J. W. Yoon, J.-S. Chang and M. S. Lah, *Chem. Commun.*, 2009, 5397–5399.
11 D. Zhao, D. Yuan, D. Sun and H.-C. Zhou, *J. Am. Chem. Soc.*, 2009, **131**, 9186–9188.
12 D. Yuan, D. Zhao, D. Sun and H.-C. Zhou, *Angew. Chem.*, 2010, **122**, 5485–5489.
13 Y. Yan, I. Telepeni, S. Yang, X. Lin, W. Kockelmann, A. Dailly, A. J. Blake, W. Lewis, G. S. Walker, D. R. Allan, S. A. Barnett, N. R. Champness and M. Schröder, *J. Am. Chem. Soc.*, 2010, **132**, 4092–4094.
14 O. K. Farha, A. O. Yazaydin, I. Eryazici, C. D. Malliakas, B. G. Hauser, M. G. Kanatzidis, S. T. Nguyen, R. Q. Snurr and J. T. Hupp, *Nat. Chem.*, 2010, **2**, 944–948.
15 B. Zheng, J. Bai, J. Duan, L. Wojtas and M. J. Zaworotko, *J. Am. Chem. Soc.*, 2011, **133**, 748–751.
16 Y. Yan, A. J. Blake, W. Lewis, S. A. Barnett, A. Dailly, N. R. Champness and M. Schröder, *Chem. – Eur. J.*, 2011, **17**, 11162–11170.
17 Y. Yan, S. Yang, A. J. Blake, W. Lewis, E. Poirier, S. A. Barnett, N. R. Champness and M. Schröder, *Chem. Commun.*, 2011, **47**, 9995–9997.
18 D. Yuan, D. Zhao and H.-C. Zhou, *Inorg. Chem.*, 2011, **50**, 10528–10530.
19 B. Li, Z. Zhang, Y. Li, K. Yao, Y. Zhu, Z. Deng, F. Yang, X. Zhou, G. Li, H. Wu, N. Nijem, Y. J. Chabal, Z. Lai, Y. Han, Z. Shi, S. Feng and J. Li, *Angew. Chem., Int. Ed.*, 2012, **51**, 1412–1415.
20 R. Luebke, J. F. Eubank, A. J. Cairns, Y. Belmabkhout, L. Wojtas and M. Eddaoudi, *Chem. Commun.*, 2012, **48**, 1455–1457.
21 B. Zheng, Z. Yang, J. Bai, Y. Li and S. Li, *Chem. Commun.*, 2012, **48**, 7025–7027.
22 I. Eryazici, O. K. Farha, B. G. Hauser, A. O. Yazaydin, A. A. Sarjeant, S. T. Nguyen and J. T. Hupp, *Cryst. Growth Des.*, 2012, **12**, 1075–1080.
23 O. K. Farha, C. E. Wilmer, I. Eryazici, B. G. Hauser, P. A. Parilla, K. O'Neill, A. A. Sarjeant, S. T. Nguyen, R. Q. Snurr and J. T. Hupp, *J. Am. Chem. Soc.*, 2012, **134**, 9860–9863.
24 O. K. Farha, I. Eryazici, N. C. Jeong, B. G. Hauser, C. E. Wilmer, A. A. Sarjeant, R. Q. Snurr, S. T. Nguyen, A. Ö. Yazaydin and J. T. Hupp, *J. Am. Chem. Soc.*, 2012, **134**, 15016–15021.
25 J. F. Eubank, F. Nouar, R. Luebke, A. J. Cairns, L. Wojtas, M. Alkordi, T. Bousquet, M. R. Hight, J. Eckert, J. P. Embs, P. A. Georgiev and M. Eddaoudi, *Angew. Chem., Int. Ed.*, 2012, **51**, 10099–10103.
26 X. Zhao, D. Sun, S. Yuan, S. Feng, R. Cao, D. Yuan, S. Wang, J. Dou and D. Sun, *Inorg. Chem.*, 2012, **51**, 10350–10355.
27 X.-J. Wang, P.-Z. Li, Y. Chen, Q. Zhang, H. Zhang, X. X. Chan, R. Ganguly, Y. Li, J. Jiang and Y. Zhao, *Sci. Rep.*, 2013, **3**, 1149.
28 Y. Yan, M. Suyetin, E. Bichoutskaia, A. J. Blake, D. R. Allan, S. A. Barnett and M. Schröder, *Chem. Sci.*, 2013, **4**, 1731–1736.
29 C. E. Wilmer, O. K. Farha, T. Yildirim, I. Eryazici, V. Krungleviciute, A. A. Sarjeant, R. Q. Snurr and J. T. Hupp, *Energy Environ. Sci.*, 2013, **6**, 1158–1163.
30 G. Barin, V. Krungleviciute, D. A. Gomez-Gualdron, A. A. Sarjeant, R. Q. Snurr, J. T. Hupp, T. Yildirim and O. K. Farha, *Chem. Mater.*, 2014, **26**, 1912–1917.

31 R. Luebke, L. J. Weselinski, Y. Belmabkhout, Z. Chen, L. Wojtas and M. Eddaoudi, *Cryst. Growth Des.*, 2014, **14**, 414–418.
32 X.-J. Wang, J. Li, P.-Z. Li, L.-B. Xing, H. Lu, H. Wu, Y. Shi, R. Zou and Y. Zhao, *Inorg. Chem. Commun.*, 2014, **46**, 13–16.
33 K. Liu, B. Li, Y. Li, X. Li, F. Yang, G. Zeng, Y. Peng, Z. Zhang, G. Li, Z. Shi, S. Feng and D. Song, *Chem. Commun.*, 2014, **50**, 5031–5033.
34 J. Li, P.-Z. Li, Q.-Y. Li, Y. Cao, H. Lu, H. Wu, F. Li, Y. Shi, X.-J. Wang and Y. Zhao, *RSC Adv.*, 2014, **4**, 53975–53980.
35 W.-Y. Gao, R. Cai, T. Pham, K. A. Forrest, A. Hogan, P. Nugent, K. Williams, L. Wojtas, R. Luebke, L. J. Weselinski, M. J. Zaworotko, B. Space, Y.-S. Chen, M. Eddaoudi, X. Shi and S. Ma, *Chem. Mater.*, 2015, **27**, 2144–2151.
36 W.-Y. Gao, T. Pham, K. A. Forrest, B. Space, L. Wojtas, Y.-S. Chen and S. Ma, *Chem. Commun.*, 2015, **51**, 9636–9639.
37 X.-J. Wang, J. Li, Q.-Y. Li, P.-Z. Li, H. Lu, Q. Lao, R. Ni, Y. Shi and Y. Zhao, *CrystEngComm*, 2015, **17**, 4632–4636.
38 Q.-Y. Li, Y. Quan, W. Wei, J. Li, H. Lu, R. Ni and X.-J. Wang, *Polyhedron*, 2015, **99**, 1–6.
39 X. Guo, Z. Zhou, C. Chen, J. Bai, C. He and C. Duan, *ACS Appl. Mater. Interfaces*, 2016, **8**, 31746–31756.
40 J. Liu, G. Liu, C. Gu, W. Liu, J. Xu, B. Li and W. Wang, *J. Mater. Chem. A*, 2016, **4**, 11630–11634.
41 S. Brunauer, P. H. Emmett and E. Teller, *J. Am. Chem. Soc.*, 1938, **60**, 309–319.
42 S. S.-Y. Chui, S. M.-F. Lo, J. P. H. Charmant, A. G. Orpen and I. D. Williams, *Science*, 1999, **283**, 1148–1150.
43 B. Chen, N. W. Ockwig, A. R. Millward, D. S. Contreras and O. M. Yaghi, *Angew. Chem., Int. Ed.*, 2005, **44**, 4745–4749.
44 V. K. Peterson, Y. Liu, C. M. Brown and C. J. Kepert, *J. Am. Chem. Soc.*, 2006, **128**, 15578–15579.
45 D. Franz, K. A. Forrest, T. Pham and B. Space, *Cryst. Growth Des.*, 2016, **16**, 6024–6032.
46 J. Eckert and W. Lohstroh, in *Neutron Applications in Materials for Energy*, ed. G. J. Kearley and V. K. Peterson, Springer International Publishing, 2015, pp. 205–239.
47 T. Pham, K. A. Forrest, B. Space and J. Eckert, *Phys. Chem. Chem. Phys.*, 2016, **18**, 17141–17158.
48 T. Pham, K. A. Forrest, J. Eckert, P. A. Georgiev, A. Mullen, R. Luebke, A. J. Cairns, Y. Belmabkhout, J. F. Eubank, K. McLaughlin, W. Lohstroh, M. Eddaoudi and B. Space, *J. Phys. Chem. C*, 2014, **118**, 439–456.
49 S. Ma, J. Eckert, P. M. Forster, J. W. Yoon, Y. K. Hwang, J.-S. Chang, C. D. Collier, J. B. Parise and H.-C. Zhou, *J. Am. Chem. Soc.*, 2008, **130**, 15896–15902.
50 C. M. Brown, Y. Liu, T. Yildirim, V. K. Peterson and C. J. Kepert, *Nanotechnology*, 2009, **20**, 204025.
51 X.-S. Wang, S. Ma, P. Forster, D. Yuan, J. Eckert, J. López, B. Murphy, J. Parise and H.-C. Zhou, *Angew. Chem., Int. Ed.*, 2008, **47**, 7263–7266.
52 T. Pham, K. A. Forrest, A. Hogan, K. McLaughlin, J. L. Belof, J. Eckert and B. Space, *J. Mater. Chem. A*, 2014, **2**, 2088–2100.
53 R. Babarao, M. Eddaoudi and J. W. Jiang, *Langmuir*, 2010, **26**, 11196–11203.
54 Y. Liu, J. F. Eubank, A. J. Cairns, J. Eckert, V. C. Kravtsov, R. Luebke and M. Eddaoudi, *Angew. Chem., Int. Ed.*, 2007, **46**, 3278–3283.
55 T. Pham, K. A. Forrest, A. Hogan, B. Tudor, K. McLaughlin, J. L. Belof, J. Eckert and B. Space, *Cryst. Growth Des.*, 2015, **15**, 1460–1471.
56 K. A. Forrest, T. Pham, K. McLaughlin, J. L. Belof, A. C. Stern, M. J. Zaworotko and B. Space, *J. Phys. Chem. C*, 2012, **116**, 15538–15549.
57 Z. Zhang, Z. Li and J. Li, *Langmuir*, 2012, **28**, 12122–12133.
58 T. Pham, K. A. Forrest, P. Nugent, Y. Belmabkhout, R. Luebke, M. Eddaoudi, M. J. Zaworotko and B. Space, *J. Phys. Chem. C*, 2013, **117**, 9340–9354.
59 T. Pham, K. A. Forrest, K. McDonald and B. Space, *Cryst. Growth Des.*, 2014, **14**, 5599–5607.
60 K. Zhang, A. Nalaparaju and J. Jiang, *J. Mater. Chem. A*, 2015, **3**, 16327–16336.
61 T. Pham, K. A. Forrest, W.-Y. Gao, S. Ma and B. Space, *ChemPhysChem*, 2015, **16**, 3170–3179.
62 N. Metropolis, A. W. Rosenbluth, M. N. Rosenbluth, A. H. Teller and E. Teller, *J. Chem. Phys.*, 1953, **21**, 1087–1092.
63 A. Z. Panagiotopoulos, *Mol. Phys.*, 1987, **61**, 813–826.
64 J. L. Belof, A. C. Stern and B. Space, *J. Chem. Theory Comput.*, 2008, **4**, 1332–1337.
65 V. Buch, *J. Chem. Phys.*, 1994, **100**, 7610–7629.
66 J. L. Belof, A. C. Stern, M. Eddaoudi and B. Space, *J. Am. Chem. Soc.*, 2007, **129**, 15202–15210.
67 G. E. Scuseria, M. D. Miller, F. Jensen and J. Geertsen, *J. Chem. Phys.*, 1991, **94**, 6660–6663.
68 J. J. Potoff and J. I. Siepmann, *AIChE J.*, 2001, **47**, 1676–1682.
69 A. L. Mullen, T. Pham, K. A. Forrest, C. R. Cioce, K. McLaughlin and B. Space, *J. Chem. Theory Comput.*, 2013, **9**, 5421–5429.
70 J.-R. Li, J. Yu, W. Lu, L.-B. Sun, J. Sculley, P. B. Balbuena and H.-C. Zhou, *Nat. Commun.*, 2013, **4**, 1538.
71 S. K. Elsaidi, M. H. Mohamed, T. Pham, T. Hussein, L. Wojtas, M. J. Zaworotko and B. Space, *Cryst. Growth Des.*, 2016, **16**, 1071–1080.
72 Y. Peng, V. Krungleviciute, I. Eryazici, J. T. Hupp, O. K. Farha and T. Yildirim, *J. Am. Chem. Soc.*, 2013, **135**, 11887–11894.
73 F. Darkrim and D. Levesque, *J. Chem. Phys.*, 1998, **109**, 4981–4984.
74 H. Wu, J. M. Simmons, G. Srinivas, W. Zhou and T. Yildirim, *J. Phys. Chem. Lett.*, 2010, **1**, 1946–1951.
75 M. J. Frisch, G. W. Trucks, H. B. Schlegel, G. E. Scuseria, M. A. Robb, J. R. Cheeseman, G. Scalmani, V. Barone, G. A. Petersson, H. Nakatsuji, X. Li, M. Caricato, A. Marenich, J. Bloino, B. G. Janesko, R. Gomperts, B. Mennucci, H. P. Hratchian, J. V. Ortiz, A. F. Izmaylov, J. L. Sonnenberg, D. Williams-Young, F. Ding, F. Lipparini, F. Egidi, J. Goings, B. Peng, A. Petrone, T. Henderson, D. Ranasinghe, V. G. Zakrzewski, J. Gao, N. Rega, G. Zheng, W. Liang, M. Hada, M. Ehara, K. Toyota, R. Fukuda, J. Hasegawa, M. Ishida, T. Nakajima, Y. Honda, O. Kitao, H. Nakai, T. Vreven, K. Throssell, J. A. Montgomery, Jr., J. E. Peralta, F. Ogliaro, M.

Bearpark, J. J. Heyd, E. Brothers, K. N. Kudin, V. N. Staroverov, T. Keith, R. Kobayashi, J. Normand, K. Raghavachari, A. Rendell, J. C. Burant, S. S. Iyengar, J. Tomasi, M. Cossi, J. M. Millam, M. Klene, C. Adamo, R. Cammi, J. W. Ochterski, R. L. Martin, K. Morokuma, O. Farkas, J. B. Foresman and D. J. Fox, *Gaussian09 Revision A.02*, Gaussian Inc., Wallingford, CT, 2016.

76 A. L. Myers and J. M. Prausnitz, *AIChE J.*, 1965, **11**, 121–127.

77 P. J. Hay and W. R. Wadt, *J. Chem. Phys.*, 1985, **82**, 270–283.

78 A. D. Becke, *J. Chem. Phys.*, 1993, **98**, 1372–1377.

79 C. Lee, W. Yang and R. G. Parr, *Phys. Rev. B: Condens. Matter Mater. Phys.*, 1988, **37**, 785–789.

80 M. Valiev, E. Bylaska, N. Govind, K. Kowalski, T. Straatsma, H. V. Dam, D. Wang, J. Nieplocha, E. Apra, T. Windus and W. de Jong, *Comput. Phys. Commun.*, 2010, **181**, 1477–1489.

81 DOE Targets for Onboard Hydrogen Storage Systems for Light-Duty Vehicles, 2012, http://energy.gov/sites/prod/files/2015/01/f19/fcto_myrdd_table_onboard_h2_storage_systems_doe_targets_ldv.pdf, Accessed on March 24, 2017.

82 ARPA-E: MOVE Program Overview, 2013, https://arpa-e.energy.gov/sites/default/files/documents/files/MOVE_ProgramOverview.pdf, Accessed on April 24, 2017.

83 D. G. Madden, H. S. Scott, A. Kumar, K.-J. Chen, R. Sanii, A. Bajpai, M. Lusi, T. Curtin, J. J. Perry and M. J. Zaworotko, *Philos. Trans. R. Soc., A*, 2017, **375**, 20160025.